

22 Figures in main text, 1 Appendix, 3 Highlighted Boxes (with 3 figures), 5 Footnotes

Chapter 4 Metabolic Fluxes

Few scientists acquainted with the chemistry of biological systems at the molecular level can avoid being inspired. Evolution has produced chemical compounds exquisitely organized to accomplish the most complicated and delicate of tasks.

Donald J. Cram

Nobel Prize Lecture, 1987

Metabolism has evolved as a complex web of intersecting biochemical pathways. Control over the flux of biochemical compounds, or *metabolites*, through these pathways requires that they be channeled in the proper direction at pathway intersections, and that they be channeled through the pathway at the proper rate. The rate at which material moves through a metabolic network can be analyzed, in theory, using assumptions about the rate by which substrates enter a pathway and the rate at which products emerge. Metabolic processing of mass and energy must follow the same thermodynamic constraints of conservation that apply to transport processes at larger scales.

Thermodynamic conservation, however, only takes us so far in being able to describe metabolic fluxes. Conservation establishes a constraint, or set of boundaries, within which quantitative descriptions of metabolism must operate. However, metabolism includes its own, unique types of complexity; those involved with network integration, adaptable control and feedback. Additionally, few metabolic pathways are expressed as isolated systems, amenable to thermodynamic constraint with well defined boundaries. Rather, they process materials and potential energy that are transferred from other pathways, and they transfer potential energy and materials to pathways beyond their boundaries. In recent decades, a new framework, called *systems biology*, has emerged from the fields of metabolic biology and biochemistry. Systems biology borrows heavily from concepts in the fields of engineering and mathematics, especially those involved with control theory and network integration. Systems biology has become differentiated, however, from its predecessors in the physical sciences, with an emphasis on molecular and genetic expression, and the means by which they provide unique and adaptable components to biological systems. These new areas of emphasis carry names like *metabolomics*

and *fluxomics* (Sweetlove and Fernie 2005, Morgenthal et al. 2006, Steuer 2007), and offer great promise to resolve some of the principle controls over the metabolic processing of mass and energy.

In this chapter we will not take up the full topic of systems biology and metabolic networks. However, there are clear lessons emerging from these fields that are relevant to the control over ecosystem-atmosphere exchanges. For example, it is becoming clear that in order to understand how the atmosphere has changed in its photochemical and radiative properties during recent periods of climate change, we must construct models with dynamic surface processes. That is, the surface processes in our models that exchange reactive and radiatively-active compounds with the atmosphere must respond dynamically to changes in climate and to feedbacks from atmospheric change. This level of dynamic control can only be introduced through simulation of those metabolic systems that process the exchanged compounds. Our discussion of metabolism will emphasize these connections between metabolic control and the uptake or emission of important constituents of the atmosphere. In particular, we will discuss the controls over photosynthetic and respiratory metabolism, the metabolic processes that largely control the exchange of CO₂ between the atmosphere and ecosystems. In addition, we will discuss metabolic control over the biosynthesis and exchange of some of the more important photochemically-active constituents of the atmosphere, such as volatile organic compounds, ammonia (NH₃) and nitrogen oxides (NO_x).

4.A The principle of shared metabolic control

Most enzymes carry out their catalytic roles within the context of metabolic pathways. Metabolic pathways consist of chains of enzyme-catalyzed reactions beginning with an overall pathway substrate and leading to a final pathway product. One of the more informative theoretical frameworks concerning the quantitative control over metabolic flux was originally derived by Kacser and Burns (1973) and Heinrich and Rapoport (1974), and is known formally as *metabolic control analysis* (MCA) (also see Crabtree and Newsholme 1987, apRees and Hill 1994, Steuer 2007). There has been debate over the years as to the relevance of the highly theoretical treatment of MCA to control over actual metabolic fluxes (e.g., Fell 1992). We will only briefly address the points of this debate in this chapter. Whether it is possible to completely reconcile MCA theory with empirical observations is not the issue on which we wish to dwell.

What we do recognize, however, is that the theory of MCA provides a useful context within which to understand how metabolic control mechanisms may operate given assumptions about optimality and the ideal allocation of enzymatic capacity. This perspective as to optimal function provides a useful measure, or starting point, from which to view actual patterns of metabolic control.

Consider a simple, hypothetical metabolic pathway (Fig. 4.1). Metabolites, or substrates, (here represented as S_1, S_2, S_3, S_4) are interspersed between coupled reactions catalyzed by a chain of enzymes (here represented as E_1, E_2, E_3) each catalyzing reactions that progress at a defined velocity (here represented as v_1, v_2, v_3). Reverse reactions are possible for each catalyzed step (here represented as v_1', v_2', v_3'). Positive or negative feedback is also possible, and is often due to allosteric interactions of the final product in the pathway on the catalytic efficiency of the first enzyme. At steady state, the net flux through each step of the pathway will equal the flux through the entire pathway (i.e., the rate at which S_4 is formed). Because each enzyme relies on the upstream reaction to provide substrate and the downstream reaction to remove product, at steady state, no single enzyme can operate faster than the entire pathway. The steps in such a pathway exhibit a high degree of *connectivity*, providing an integrated, systemic nature that reflects the articulated contributions of its individual reactions.

Perturbation to the velocity of any single reaction in the pathway will be transmitted through the system until a new steady state is reached. Consider a hypothetical perturbation whereby v_1 is increased. This would cause the concentration of S_2 to increase, causing v_2 to also increase. The increase in v_2 , however, will eventually reach a limit. It will only be able to increase to a velocity equal to the new v_1 . At that point, the flux through E_1 and E_2 will be at a new steady state and the concentration of S_2 will become constant again. This same effect will be transmitted down the line until all velocities in the pathway settle on the new steady state. One important assumption required for this scenario is that the pathways upstream from S_1 and downstream from S_4 must be operating such that the concentrations of S_1 and S_4 remain sufficient and constant in the face of perturbation to v_1 . In other words, boundary conditions for the pathway must not limit its flux.

Despite equality in steady-state reaction rate, every enzyme in a pathway does not exert the same degree of control over flux. The amount of control exerted by an enzyme can be quantified as the degree to which a perturbation in the activity of the enzyme (or concentration of the

enzyme) affects total flux through the pathway. Expressed formally, this relationship defines the flux control coefficient (C_{E_x}).

$$C_{E_x} = \frac{\partial F/F}{\partial c_{E_x}/c_{E_x}} \quad (4.1)$$

where F is the total flux rate through the pathway and c_{E_x} is the concentration of a specific enzyme in the pathway (e.g., E_1 , E_2 , E_3 , etc.). By convention, the nomenclature of C_{E_x} is such that the subscript refers to enzyme x (denoted as E_x), where x represents any sequential enzyme in the pathway, e.g., 1, 2, 3, etc. Because the relationship described in Equation 4.1 is defined in terms of a fractional change in pathway flux, control coefficients are dimensionless.¹

The flux control coefficient is dependent on two components of flux. The *local* flux is defined by the individual response of an enzyme to the milieu of metabolites that surround it, and the *systemic* flux as defined by the connected influences of one enzyme's control coefficient on those of other enzymes (Fell 1992). Local control over flux is ultimately expressed through characteristics of the active and regulatory sites of an enzyme (e.g., the substrate binding affinity, the sensitivity of that binding affinity to allosteric regulation, and the enzyme turnover number). These properties underlie the elasticity coefficient ($\varepsilon_j^{v_x}$):

$$\varepsilon_j^{v_x} = \frac{\partial v_x/v_x}{\partial c_j/c_j} \quad (4.2)$$

where c_j represents the concentration of some metabolite (j) with which the enzyme associates. The nomenclature for the elasticity coefficient, $\varepsilon_j^{v_x}$, follows convention whereby the superscript refers to the velocity of the specific reaction being characterized and the subscript refers to the metabolite being considered. The elasticity coefficient is an expression of the relative change in reaction velocity given a change in metabolite concentration, holding all other metabolite concentrations constant. It should be noted that both C_{E_x} and $\varepsilon_j^{v_x}$ are defined as partial derivatives, whereby the fractional changes in pathway flux (F) or enzyme velocity (v) are defined in the limit as fractional changes in the concentrations of enzyme x (c_{E_x}) or metabolite j

(c_j) become infinitesimally small. Like C_{Ex} , $\varepsilon_j^{v_x}$ is dimensionless and its value will vary from 0 to 1.

Systemic control over flux is expressed through the combined influences of the flux control coefficients of all enzymes in a pathway. Given the systemic nature of shared control, it might be expected that all flux control coefficients would sum to a limit. Additionally, given the fractional nature of the flux control coefficient, it might be expected that the limit would be defined within the context of $\partial F/F$. In fact, it can be shown that for any given pathway, the flux control coefficients for the entire pathway must sum to a limit when $\partial F/F = 1$. This is expressed formally as the summation theorem:

$$\sum_{x=1}^n C_{Ex} = 1 \quad (4.3)$$

where C_{Ex} represents the control coefficient for each successive enzyme in the pathway, and n is the total number of enzymes in the pathway. Thus, if an enzyme exhibits a flux control coefficient of 0.45, it exerts 45% of the control over flux through the pathway. The summation theorem makes clear one of the fundamental tenets of metabolic control analysis. That is, control over flux is potentially *shared* among all the enzymes of a pathway. A derivation of the summation theorem is provided in Appendix 4.1.

From Equations 4.2 and 4.3 it is clear that a required interdependence exists between the systemic properties of pathway flux, as represented by the control coefficient, and the local properties of enzymatic function, as represented by the elasticity coefficient. Using this concept of interdependence, one can define a formal relationship between C_{Ex} and $\varepsilon_j^{v_x}$ for sequential reactions that share common metabolites:

$$\frac{C_{E1}}{C_{E2}} = \frac{|\varepsilon_2^2|}{|\varepsilon_2^1|} \quad (4.4)$$

where C_{E1} and C_{E2} are the control coefficients for two successive enzymes in a pathway (E_1 and E_2 in Equation 4.5), and ε_j^1 and ε_j^2 refer to the elasticity coefficients for the reverse reaction of

E_1 (indicated as v_1' in Equation 3.5) and forward reaction of E_2 (indicated as v_2 in Equation 5.5), respectively, with respect to a single shared metabolite S_2 .



Equation 4.4 is known as the *connectivity theorem*. The connectivity theorem reveals that there is an inverse, proportional relationship between the control coefficient for an enzyme and its elasticity coefficient with respect to substrate. Greater control over pathway flux comes with a greater tendency to resist changes in substrate concentrations. Taking this interpretation a bit further, enzymes with higher control coefficients tend to be less sensitive to *mass action influences* (i.e., the influence of disequilibrium caused by the ratio of product to substrate). A derivation of the connectivity theorem is presented in Appendix 4.1.

The quantitative framework of MCA emphasizes shared control among all enzymes in a pathway. In every case to date where MCA has been applied to a specific pathway, calculated control coefficients are less than 1 for each step, indicating shared control. The theoretical underpinnings of MCA do not, however, require *equal* sharing. In most cases where MCA has been applied, the calculated control coefficients are high for relatively few enzymes, and in some cases approaches 1 for a single enzyme. Thus, control may indeed be shared, but it is unequally shared, and to a large extent focused on traditionally identified rate-limiting steps (see Atkinson 1990).

Under the forces of natural evolution, the structural and functional design of organisms is channeled toward outcomes that optimally utilize limited, available resources and thus maximize reproductive fitness (see Bloom et al. 1985). This may explain why most metabolic pathways exhibit unequal sharing and why control is focused on relatively few steps. To illustrate this point, imagine a pathway in which control is equally shared among all steps. Now, imagine that there is a selective advantage to increased flux through the pathway, but limited access to the resources (e.g., nitrogen) required to increase the concentration of all enzymes equally. The greatest marginal gains in flux will occur by investment of the limiting resource in producing more of those enzymes with the highest catalytic potential per unit of resource, leaving those

enzymes with the lowest catalytic potential per unit of resource as the most rate-limiting steps with the highest potential for control over flux (Woodrow and Mott 1993). This is one evolutionary explanation for connectivity among steps in a pathway. The concept of unequal sharing will become even clearer as we consider Metabolic Control Analysis within the context of photosynthetic CO₂ assimilation, one of the more thoroughly characterized metabolic processes in plants.

4.B Photosynthetic metabolism

Few pathways are as crucial to understanding the metabolic regulation of ecosystem-atmosphere interactions as that for photosynthetic CO₂ assimilation. Photosynthesis is controlled at a number of scales, including those within leaves, cells and chloroplasts. In this chapter, we will be most concerned with interactions at the chloroplast level (Fig. 4.2). Higher levels of control will be considered in future chapters on leaf, canopy and ecosystem processes.

4.B.1 The biochemistry of photosynthetic CO₂ assimilation

Photosynthetic CO₂ assimilation depends on the interaction between photon-assimilating and CO₂-assimilating reactions which occur in different parts of the chloroplast (Fig. 4.3). Through this interaction the quantized energy carried in solar photons is used to synthesize adenosine triphosphate (ATP) molecules and chemically reduce the compound nicotinamide-adenine dinucleotide phosphate (NADP⁺). Ultimately, the energy is used to convert CO₂ molecules into sugar-phosphate molecules. The electrons that participate in the C-O bonds of CO₂ exist at a low potential energy level due to the high electronegativity of O. The enzymatic conversion of CO₂ to a sugar-phosphate requires an increase in the free energy of the electrons by approximately 3 kcal mol⁻¹. This increase in chemical free energy comes at the expense of absorbed solar energy.

The rates at which the photon-assimilating and CO₂-assimilating pathways are permitted to operate are constrained by their dependence on one another. The CO₂-assimilating pathway can only operate as fast as the photon-assimilating pathway provides it with ATP and NADPH. The photon assimilating pathway can only operate as fast as the CO₂-assimilating pathway returns NADP⁺, ADP and inorganic phosphate (P_i) to act as electron and free energy acceptors. The photon-assimilating reactions are composed of (1) *light-harvesting components* (including the

chlorophyll pigments), which absorb photons of light and use the energy to excite electrons, and (2) *electron-transport components*, which facilitate transfer of the excited electrons across membranes, causing the synthesis of ATP, and ultimately NADPH. In sum, the photon-assimilating reactions: (1) oxidatively extract two electrons with relatively low potential energy from H₂O (stoichiometrically producing 1/2 of an O₂ molecule), (2) energize the two electrons using photons of light and engaging two different light-harvesting photosystems, and (3) reductively pass the energized electrons to an electron donor molecule, NADP⁺, thus forming NADPH. The electrons carried in NADPH exist at a relatively high potential energy level. In the process of moving the electrons from H₂O to NADP⁺, some of the energy from the absorbed photons is extracted, used to conduct work, and synthesize ATP.

The CO₂-assimilating reactions are known variably as the reductive pentose phosphate pathway, the C₃ pathway, or the Calvin-Benson cycle. In this book, these reactions will be referred to as the *reductive pentose phosphate pathway*, or RPP pathway (Fig. 4.4). The overall result of the RPP pathway is that one triose-phosphate sugar is produced as a net gain for every three molecules of assimilated CO₂. The initial assimilation of CO₂ occurs through a reaction catalyzed by the enzyme RuBP carboxylase/oxygenase (Rubisco) (represented by step 1 in Fig. 4.4) which resides in the soluble stroma of the chloroplast. In this initial reaction, Rubisco facilitates the formation of a covalent bond between CO₂ and a 5-carbon acceptor molecule, ribulose 1,5-bisphosphate (RuBP). The stable product of the Rubisco-catalyzed reaction is two molecules of the three-carbon compound, 3-phosphoglyceric acid (PGA); thus, the title 'C₃-cycle' that is often provided to the pathway. Following the initial assimilation of CO₂, other enzymes in the pathway utilize ATP and NADPH from the photon-assimilating reactions to chemically reduce PGA to form glyceraldehyde 3-phosphate (G3P), a triose-phosphate sugar (represented by steps 2 and 3). Some of the triose-phosphate sugar is exported from the chloroplast to produce sucrose in the cytoplasm, and releasing inorganic phosphate (Pi), which can be transported back into the chloroplast for further use (represented by step 4). The remaining triose phosphate molecules are restructured in a series of enzyme-catalyzed reactions to form a variety of intermediate compounds, eventually reforming RuBP, the original CO₂ acceptor, at the expense of another ATP molecule (represented by step 6). Thus, the RPP pathway is truly 'cyclic' in the sense that the original 5-carbon acceptor of CO₂ (RuBP) is ultimately regenerated. The maintenance of flux through the cycle requires the proper

partitioning of sugar phosphate product between the export (to form sucrose) and regenerative (to form RuBP) phases of process. The entire cycle is driven by the ATP energy and NADPH reductive potential provided by solar energy through the photon-assimilating reactions (see Woodrow and Berry 1988 for a review of the primary controls over flux through the RPP pathway). Plants that use the RPP pathway as the means to assimilate CO₂ directly from the atmosphere are often referred to as C₃ plants.

4.B.2 The transfer of CO₂ between the gaseous (atmospheric) and aqueous (cellular) phases

Photosynthetic fluxes require the transfer of CO₂ molecules from the gaseous phase in the atmosphere to the aqueous phase of leaf photosynthetic cells, and ultimately to the active site of Rubisco in the chloroplast. Dissolved CO₂ is the primary substrate that enters the RPP pathway. Gases dissolve in cells according to Henry's Law. At equilibrium, Henry's Law predicts that the density of a constituent that dissolves in the aqueous phase is proportional to its partial pressure in the surrounding gas phase. At a constant temperature, the concentration of CO₂ dissolved in water [$c_{c(w)}$] is directly proportional to the partial pressure of CO₂ in the adjacent air phase [$P_{c(a)}$]:

$$c_{c(w)} = P_{c(a)} / k_H \quad (4.6)$$

where k_H is the Henry's Law constant for CO₂. When written in the form of Equation 4.6 and at 25°C, k_H carries the value of 29.4 x 10² kPa mol l⁻¹. As the temperature of a leaf increases, k_H decreases, and the concentration of dissolved CO₂ in the cell also decreases.

Once in the cell, some fraction of the CO₂ reacts with water, forming bicarbonate according to $CO_{2(w)} + H_2O \rightleftharpoons HCO_3^- + H^+ \rightleftharpoons CO_3^{2-} + 2H^+$. The dissociation reactions on the right-hand side of the equation are near-instantaneous. The hydration-dehydration reactions on the left-hand side of the equation are relatively slow. The final equilibrium with respect to CO₂ and HCO₃⁻ depends on pH, favoring CO₂ at acidic pH and HCO₃⁻ at basic pH (at pH 6 approximately 75% of the total inorganic carbon exists as CO₂ and at pH 8 approximately 80% of the total inorganic carbon exists as HCO₃⁻). The stroma of the chloroplast, where CO₂ is assimilated, typically exists at a pH near 8 in light, meaning that most of the inorganic carbon exists as HCO₃⁻. Given this situation, the conversion of HCO₃⁻ to CO_{2(w)} plus H₂O, and subsequent

diffusion of CO₂ to the active site of Rubisco, is a potentially rate-limiting process in C₃ photosynthesis. Presumably to relieve this limitation, catalytic potential has evolved in the form of *carbonic anhydrase*, a zinc-containing enzyme capable of accelerating the CO₂/HCO₃⁻ equilibrium. Carbonic anhydrase occurs at relatively high activities in the chloroplasts of C₃ photosynthetic cells where it facilitates high rates of Rubisco carboxylation through the conversion of HCO₃⁻ to CO_{2(w)} in the vicinity of the Rubisco active site.

4.B.3 The nature of Rubisco

The entrance of CO₂ into the RPP pathway occurs by way of Rubisco. As enzymes go, Rubisco is large. It is composed of eight 'large' subunits encoded by chloroplast genes, and eight 'small' subunits encoded by nuclear genes. Each large subunit contains an active site and allosteric regulatory sites. The small subunits are not catalytically active, but rather modify the activity of the large subunits. As enzymes go, Rubisco is also inefficient, at least with regard to the current atmospheric CO₂ concentration (Morell et al. 1992). The active site of Rubisco assimilates CO₂ with a Michaelis-Menten coefficient (analogous to the K_m , see Section 3.C.1, but often denoted as K_C) that is slightly less than the current atmospheric CO₂ concentration. The CO₂ concentration in the chloroplast is even less than that in the atmosphere due to diffusive resistances between the atmosphere and chloroplast. This means that under normal conditions, Rubisco is functioning at less than half its maximum velocity. Additionally, the turnover rate at each active site of Rubisco is slow (approximately 1-3 conversions per second depending on temperature and CO₂ concentration). The large size and inefficient catalytic function of Rubisco, along with its central role in assimilating CO₂, requires that large amounts of nitrogen be allocated to this single protein in order to sustain rates of CO₂ assimilation adequate for plant growth. In C₃ plants, up to 35% of a leaf's N can be tied up in Rubisco. In pure crystalline form, Rubisco active sites exist at a concentration of approximately 10 mM. In a typical C₃ chloroplast, Rubisco active sites exist at a concentration of 1-4 mM. Although some storage proteins exist at such high concentrations, it is rare to find catalytic proteins at such high concentrations. For a review of Rubisco, including its structural and regulatory properties, see Spreitzer and Salvucci (2002).

Rubisco is a highly regulated enzyme as might be expected given its role as the 'gatekeeper' to photosynthetic CO₂ assimilation. Rubisco exists in active and inactive states.

The inactive form is converted to the active form through the activity of an ATP-dependent regulatory enzyme, *Rubisco activase*, followed by the addition of a CO₂ molecule (carbamylation) to a critical amino acid residue in the active site, and finally the addition of a Mg²⁺ ion to the active site as a second effector. The bound Mg²⁺ ion is required to properly activate RuBP substrate and stabilize the transition state during catalysis. When both the CO₂ and Mg²⁺ effectors are present, the enzyme is in the final active form. The active form has a finite lifetime and will spontaneously revert to the inactive form when the carbamylated lysine loses its CO₂ after several catalytic cycles. The complex activation of Rubisco serves the important regulatory role of activating photosynthetic CO₂ assimilation only under conditions when the photon-assimilating reactions are active, providing ATP for the initial step in activation, catalysis by Rubisco activase.

Once active, RuBP substrate is coordinated to the Mg²⁺ ion in the active site of Rubisco. Binding of RuBP, and the strain placed on its bonds as it coordinates with the Mg²⁺ and carbamylated lysine, causes it to deprotonate form a reactive *enediolate intermediate structure*. The intermediate is receptive to forming a new covalent bond with a substrate CO₂ molecule, thus initiating CO₂ assimilation (see Lorimer et al. 1993). In some cases, the enediolate intermediate forms a bond with O₂, rather than CO₂. The potential for RuBP in the active site of Rubisco to form a bond with O₂ explains the word 'oxygenase', as the final nomenclatural component of ribulose 1,5-bisphosphate carboxylase/oxygenase (i.e., the 'O' in Rubisco; see Ogren 2003 and Portis and Parry 2007 for historical reviews of the discovery of oxygenase activity in Rubisco).

As substrates, CO₂ and O₂ react competitively with the enediolate intermediate at Rubisco's active site. However, the catalytic affinity for CO₂ ($K_C = 300 \mu\text{mol mol}^{-1}$ at 25°C) is considerably higher than that for O₂ ($K_O = 420 \text{mmol mol}^{-1}$ at 25°C). The maximum rate of oxygenation catalyzed by Rubisco is approximately 25% the maximum rate of carboxylation. Thus, the rate of oxygenation can approach the rate of carboxylation only in circumstances when the CO₂ concentration is quite low compared to the O₂ concentration. For plants that utilize the RPP pathway to assimilate CO₂ in the normal atmosphere (~380 $\mu\text{mol mol}^{-1}$ CO₂, 210 mmol mol^{-1} O₂), and at moderate temperatures (25-30 °C), carboxylation proceeds at 4-5 times the rate of oxygenation.

The degree to which the active site of Rubisco favors carboxylation over oxygenation can be assessed through a ratio of the relative kinetic parameters governing both reactions. The *relative specificity* of Rubisco activity for CO₂ versus O₂ (denoted as S_{rel}) is expressed as:

$$S_{\text{rel}} = \frac{V_{\text{cmax}} K_o}{V_{\text{omax}} K_c} \quad (4.7)$$

where V_{omax} and V_{cmax} are the maximum rates of oxygenation and carboxylation by Rubisco.² During the past history of the earth, terrestrial plants have evolved changes in the active site of Rubisco that allow S_{rel} to track changes in atmospheric CO₂ concentration (Jordan and Ogren 1981). Current models suggest that the earth's atmosphere contained CO₂ concentrations that were many times higher than today's atmosphere and O₂ concentrations that were low until approximately 2-3 billion years ago. Rubisco from cyanobacteria, which retains many aspects of the primitive state of the enzyme, exhibits an S_{rel} value of 40-60. Rubisco from terrestrial C₃ plants, which reflects evolutionary change since atmospheric CO₂ concentrations have decreased and O₂ concentrations have increased, exhibits an S_{rel} value of 75-85. Thus, the active site of Rubisco has evolved in a way that increases its capacity to assimilate CO₂ relative to O₂, and this has compensated at least partly for historical changes in atmospheric composition.

It's important to note that the active site does not actually bind the substrate CO₂ molecule and transfer it to the enediolate intermediate. In fact, as a biochemical entity, the CO₂ molecule has few properties (e.g., polarity, asymmetric structure) which might be 'used' by an active site to form a properly bound enzyme-substrate complex; what is often called in biochemistry, a proper 'Michaelis-Menten complex'. In the words of some researchers, the CO₂ molecule is biochemically 'featureless' (Pierce et al. 1986, Tcherkez et al. 2006). This means the only catalytic mechanism by which Rubisco can favor carboxylation of the enediolate intermediate, and deter reaction with other electrophilic constituents of the atmosphere, is through the placement of amino acid side chains in the active site that favor the transition state that is formed following carboxylation compared to, for example, oxygenation. A thermodynamic analysis, however, has revealed that stabilization of the carboxyketone form of the carboxylated transition state, requires such tight binding to the active site that it slows cleavage of the transition state to form the ultimate three-carbon products (two PGA molecules) (Tchkerz et al. 2006). Thus,

evolution of the Rubisco active site has encountered a trade-off between 'favoring' CO₂ substrate and turning over the carboxylated transition state to form and release product (see Section 3.C.1 for a discussion of tradeoffs and compromises in enzyme K_m and k_{cat}). The fact that many enzymes from different types of photosynthetic organisms have converged on similar active site mechanisms suggests that there is a design to optimally accommodate this trade-off, producing a Rubisco enzyme that is capable of relatively high specificity for CO₂ in an atmosphere dominated by O₂, but necessarily slow (see Gutteridge and Pierce 2006).

Temperature is known to have a strong influence on the relative rates of carboxylation and oxygenation catalyzed by Rubisco. An increase in temperature causes a decrease in S_{rel} , which favors oxygenation relative to carboxylation. The temperature effect is due to greater reductions in the active site affinity of Rubisco for CO₂ relative to O₂ (i.e., greater increase in K_c relative K_o) as temperature increases (Fig. 4.5). Additionally, the solubility of CO₂ decreases to a greater extent than the solubility of O₂ as temperature increases.

The metabolic product of each oxygenation reaction at the active site of Rubisco is one molecule of PGA (which is processed through the RPP pathway just as for the PGA produced by carboxylation) and one molecule of the two-carbon molecule, phosphoglycolate (PGL). In terrestrial plants, an independent metabolic pathway involving three different cellular organelles (chloroplasts, peroxisomes and mitochondria) has evolved to process the PGL (Fig. 4.6). This pathway is often referred to as *photorespiration*. Through photorespiration, three-quarters of the carbon contained in PGL are converted to PGA which then enters the RPP pathway (Fig. 4.7). Thus, photorespiration can be viewed as a carbon recovery process that is capable of recycling much of the carbon contained in the products of oxygenation. The recovery is advantageous to the carbon balance of the plant, but it is not ideal in that one-quarter of the carbon contained in the PGL is lost as CO₂. Additionally, for every oxygenation, 3.5 ATP and 2 NADPH reducing equivalents are utilized in the recycling of the photorespiratory metabolites. In the overall balance, the oxygenation of RuBP and subsequent photorespiratory metabolism is costly to the plant, both in terms of energy and reduced carbon. For a further discussion of photorespiratory metabolism see Douce and Heldt (2000). With the understanding that the exchange of CO₂ across C₃ plant leaves involves both CO₂ assimilation through the RPP pathway and CO₂ loss through the photorespiratory pathway (as well as mitochondrial respiration of the TCA cycle,

which will be discussed shortly), we can define *net CO₂ assimilation rate* as the difference between the gross rates of CO₂ uptake and loss.

Plant photorespiration is relevant to ecosystem-atmosphere interactions within the context of future climate warming. The temperature dependent changes in S_{rel} , which were discussed above, can explain the increase in photorespiration rate and decrease in net CO₂ assimilation rate as the temperature of C₃ plant leaves increases (Fig. 4.8). The effects of temperature on photorespiration and photosynthesis are especially obvious at low atmospheric CO₂ concentrations, and these effects are mitigated as the atmospheric CO₂ concentration increases. The effect of increasing temperature and CO₂ concentration on the kinetic characteristics of Rubisco provides a mechanistic understanding for why we expect global photosynthesis rates to change in the face of a changing climate and increases in atmospheric CO₂ concentration due to fossil fuel usage.

4.B.4 The evaluation of photosynthetic CO₂ assimilation using Metabolic Control Analysis

Metabolic Control Analysis has been applied to the RPP pathway in a handful of cases (Woodrow 1986, Giersch et al. 1990, Stitt 1996, Poolman et al. 2000). In each case, the application has not been ideal and the strictest tenets of MCA have been violated to some extent. For example, in the chloroplast, the RuBP concentration (0.5 - 8 mM) is similar to the concentration of Rubisco active sites (1 - 4 mM). Thus, in the RPP pathway, RuBP substrate can limit the overall rate of pathway flux, in addition to the concentrations of component enzymes. This causes violation of one of the central conditions of MCA; that the rate of catalysis be proportional in the first order to the concentration of enzyme. In a second violation, the requirement in MCA that boundary conditions not constrain pathway flux comes into play. Recall that in MCA, the flux rate must be controlled solely by the concentrations of the component enzymes, not by the rate of entry of substrates or other metabolites from outside the pathway. In the chloroplast, there are conditions in which the availability of inorganic phosphate (P_i) limits flux through the RPP pathway. In its purest form, MCA cannot accommodate this condition. In past efforts to apply MCA to the RPP pathway, researchers have found ways to relax the theory and accommodate these points of violation.

The studies described here with regard to the calculation of flux control coefficients for the RPP pathway were conducted with computer models. Empirically-derived data exists for the

stromal concentration of some RPP pathway metabolites, such as RuBP, PGA, SBP, F6P and G6P. Other information, such as the overall rate of net CO₂ assimilation and the concentration of Rubisco active sites, is also fairly well known. These few measurements can be entered into a model to establish some initial quantitative boundaries within which the model must operate. Then the concentrations and fluxes of other unknown steps can be estimated. In applications of this approach, a rather detailed step-by-step model of the RPP pathway is used, with the fundamental framework following the tenets of Metabolic Control Analysis (e.g., Woodrow and Mott 1993).

In the presence of an atmospheric CO₂ concentration typical of the last few decades, control over flux is focused on one enzyme, Rubisco (Fig. 4.9). In this condition, the control coefficient for carboxylation by Rubisco approaches unity. Smaller, positive control contributions are provided by stromal fructose 1,6-bisphosphatase and the synthesis of sucrose from triose-phosphate sugars in the cytoplasm. The oxygenase activity of Rubisco exerts negative control, meaning that the velocity of the net CO₂ assimilation rate decreases as the velocity of the oxygenase reaction increases. The negative contribution by ATPase reflects progressively greater sequestration of P_i in the ATP metabolite pool as ATPase activity increases. This would limit the potential to export sugar-P compounds from the chloroplast and lead to feedback inhibition of the CO₂ assimilation rate. An increase in the activity of those enzymes that exhibit positive control coefficients would, by definition, cause an increase in flux through the RPP pathway, although to differing degrees. An increase in the activity of those with negative control coefficients would cause a reduction in flux through the RPP pathway.

The high degree of control by Rubisco is sensitive to the availability of the CO₂ and RuBP substrate concentrations (Collatz et al. 1990). As CO₂ concentration is increased, the velocity of the CO₂ assimilation rate will increase, the availability of RuBP will decrease, and carboxylation rate will be progressively constrained by RuBP availability (Fig. 4.10). As CO₂ concentration increases a shift occurs in the calculated control coefficients of the RPP pathway from a state of dominant control by Rubisco to a state of dominant control by other enzymes, particularly those that control the rate RuBP regeneration (Fig. 4.11). For example, the enzyme ribulose 5-phosphate (Ru5P) kinase, which catalyzes the synthesis of RuBP, exhibits a higher control coefficient as CO₂ concentration increases and RuBP concentration decreases, and Rubisco exhibits a lower control coefficient (Fig. 4.12). The connectivity among steps in a metabolic

pathway, as expressed in MCA, is seen clearly in this switch from dominant control by one enzyme to that of another enzyme as one substrate becomes more limiting than another.

One interesting control dynamic is evident in the large swing in the control coefficient of sucrose synthesis, from negative to positive, as a result of changes in RuBP concentration (see Fig. 4.11). When RuBP concentration is low, an increase in sucrose synthesis rate will cause a decrease in flux through the RPP pathway. This is due to the fact that sucrose synthesis, which occurs in the cytosol, releases P_i that is then free to be transported back into the chloroplast in exchange for triose-P sugars (see step 4 in Figure 4.4). The outward flux of triose-P sugars drains the chloroplast of substrate that is needed to regenerate RuBP, and provides the basis for the negative control coefficient. At high RuBP concentrations, carbon substrate is not as likely to limit the rate of RPP flux as is P_i (which is tied up in the RuBP pool). Thus, an increase in sucrose synthesis at high concentrations of RuBP will provide a supply of rate-limiting P_i to be transported back into the chloroplast and increase flux through the RPP pathway; providing the basis for the positive control coefficient. A similar control scenario can be provided for starch synthesis, although in that case all processes reside within the chloroplast.

4.C A simplified biochemical model of CO₂ assimilation rate

It is perhaps a matter of taste, but I find analytical solutions, as opposed to numerical ones, more enlightening. Unfortunately, the complexity of photosynthesis means that analytical descriptions can only be achieved at the expense of gross simplification... (these models) can be useful aids to understanding, and for prediction, but are also potential hazards when the simplifications involved are forgotten.

Graham Farquhar (1989)

Modeling a process as complex as photosynthesis from the first principles of reaction rate coefficients, metabolite pool sizes and chloroplast enzyme concentrations proved to be an exceptional challenge a few decades ago to those researchers brave enough to confront the issue (see Peisker 1974, Laisk 1977, Hall 1979). As observations of variability in CO₂ assimilation rate became available for a broad range of environmental conditions, and knowledge emerged about the role of Rubisco as a primary control over CO₂ assimilation rate, modeling strategies switched from numerical descriptions of multiple sequential reactions, to analytical descriptions that folded the integrated interactions of multiple photosynthetic processes into two fundamental,

rate-limiting conditions (see Farquhar et al. 1980b). In this analytical perspective, it was recognized that the rate of CO₂ assimilation could only go as fast as the capacity for Rubisco to catalyze the carboxylation reaction and the capacity for the electron transport reactions to support RuBP production. As described in a published, but abbreviated, history of photosynthetic modeling (Farquhar et al. 2001), in the late 1970's, Graham Farquhar, Suzanne von Caemmerer and Joe Berry, came to recognize the process of CO₂ assimilation as 'see-sawing' back and forth between these two limitations depending on the photon flux (which drives the production of RuBP) and the chloroplast CO₂ and O₂ concentrations (which determine Rubisco catalytic activity). In later studies, a third limiting case was added, that involving inorganic phosphate (P_i) availability, especially at high chloroplast CO₂ concentrations. The most widely accepted models of the RPP pathway are still based on these three assumed fundamental controls. Stated explicitly, the primary control over RPP flux is modeled as the minimum of three photosynthetic states: (1) the *Rubisco-limited state*, in which the availability of CO₂ and the kinetic properties of the active site of Rubisco limit the flux, (2) the *RuBP-limited state*, in which the rate of RuBP production limits the flux (i.e., the rate at which ATP and NADPH can be utilized to regenerate RuBP), and (3) the *triose-phosphate utilization (TPU)-limited state*, in which the rate of P_i recycling limits the rate of ATP biosynthesis (Fig. 4.13).

The interaction of these constraints can be illustrated through a graph of the rate of RuBP carboxylation plotted against the CO₂ concentration (c_{cc}) or the photosynthetic photon flux density (PPFD) in the chloroplast (Fig. 4.14). In assessing the response pattern in the upper panel of Figure 4.14, at low c_{cc} and high PPFD, the catalytic activity of Rubisco represents the principal limitation to the overall rate of CO₂ assimilation. As c_{cc} increases, RuBP availability takes over as the principal limitation. At high c_{cc} , the rate of carboxylation will exceed the rate of triose-phosphate utilization, and the third limitation, the rate at which P_i is recycled becomes the principal limitation. In assessing the response pattern in the lower panel, the rate of carboxylation at low PPFD is limited by the rate of RuBP production. As PPFD increases, RuBP regeneration capacity becomes less of a limitation and the capacity of Rubisco to utilize its other substrate, CO₂ becomes more of a limitation. Thus, in assessing both panels together, the carboxylation rate at any given c_{cc} or PPFD is assumed to be controlled by the greater of three possible constraints.

4.C.1 Modeling the Rubisco-limited state

The Rubisco-limited state of photosynthesis is realized when RuBP is available to Rubisco in rate-saturating amounts. In this case, it is the reaction rate of the second substrate, CO₂, which determines the rate of carboxylation. Following the general form of the Michaelis-Menten model of enzyme kinetics, the rate of RuBP carboxylation can be represented as:

$$v_{c1} = \frac{V_{\text{cmax}} c_{\text{cc}}}{c_{\text{cc}} + K_c (1 + c_{\text{oc}}/K_o)} \quad (4.8)$$

where v_{c1} represents the rate of carboxylation ($\mu\text{mol CO}_2 \text{ m}^{-2} \text{ leaf area s}^{-1}$) in the presence of unlimited RuBP supply, V_{cmax} is the maximum velocity of carboxylation ($\mu\text{mol CO}_2 \text{ m}^{-2} \text{ leaf area s}^{-1}$), c_{cc} is the mole fraction of CO₂ in the chloroplast at the active site of Rubisco ($\text{mol CO}_2 \text{ mol}^{-1} \text{ air}$), K_c is the Michaelis-Menten coefficient describing the affinity of the active site for CO₂ (analogous to the K_m with respect to CO₂) ($\text{mol CO}_2 \text{ mol}^{-1} \text{ air}$), c_{oc} is the mol fraction of O₂ in the chloroplast at the active site of Rubisco ($\text{mol O}_2 \text{ mol}^{-1} \text{ air}$), and K_o is the Michaelis-Menten coefficient describing the affinity of the Rubisco active site for O₂ ($\text{mol O}_2 \text{ mol}^{-1} \text{ air}$). The term $(1 + c_{\text{oc}}/K_o)$ modifies K_c according to the presence of a competitive inhibitor. In the presence of O₂, the affinity of the active site for CO₂ decreases (i.e., K_c increases). Equation 4.8 is expressed in terms of a unit of leaf area (m^{-2}) and with mole fractions of CO₂ and O₂ referenced to air. By expressing the relations on these bases, the model can be applied to prediction of the net CO₂ assimilation rate of intact C₃ leaves and in relation to atmospheric CO₂ and O₂ concentrations.

Until recently, the Michaelis-Menten coefficients for CO₂ and O₂ that were available for the purposes of modeling were determined from *in vitro* assays of extracted Rubisco which, by necessity, were conducted in test tubes in a relatively diluted state. In the chloroplast, however, Rubisco occurs in a more concentrated state. The question as to the relevance of kinetic coefficients determined *in vitro* to the *in vivo* condition has remained open to debate. Using genetically-engineered tobacco plants, von Caemmerer et al. (1994) were able to reduce the Rubisco content of leaves and approximate the diluted state that has been studied *in vitro*. Kinetic characterization of the transgenic plants confirmed that the Michaelis-Menten coefficients of Rubisco determined from *in vitro* studies are similar to those derived from diluted *in vivo* measurements.

4.C.2 Modeling the RuBP-limited state

In the presence of high c_{cc} or low PPFD the rate of net CO_2 assimilation is limited by the rate at which RuBP is regenerated in the RPP pathway, utilizing the ATP and NADPH produced by the chloroplast electron transport chain. In general terms, the degree to which electron transport capacity limits the rate of carboxylation (v_{c2}) can be expressed as follows (from Farquhar et al. 1980b):

$$v_{c2} = \frac{\text{rate of electron transport}}{\text{amount of electron transport required to regenerate RuBP}} \quad (4.9)$$

The development of a quantitative model from this conceptual relation requires consideration of the amount of NADPH or ATP consumed in converting two moles of PGA to one mole of RuBP. For simplicity, we will derive the model on the basis of NADPH consumption.³

The rate of NADPH consumption will equal the rate of PGA production plus the rate at which NH_4^+ is re-assimilated from the photorespiratory process (see Figs. 4.6 and 4.7). Each mole of PGA requires one mole of NADPH for reduction to triose phosphate, and each mole of NH_4^+ ion requires one mole of NADPH for re-assimilation into the amino acid pool of the cell. Following these assumptions, the rate of PGA production ($\text{mol PGA m}^{-2} \text{ leaf area s}^{-1}$) can be expressed as:

$$\text{rate of PGA production} = 2v_c + 1.5 v_o \quad (4.10)$$

where v_c is the rate of Rubisco-catalyzed carboxylation ($\text{mol CO}_2 \text{ m}^{-2} \text{ leaf area s}^{-1}$) and v_o is the rate of Rubisco-catalyzed oxygenation ($\text{mol O}_2 \text{ m}^{-2} \text{ leaf area s}^{-1}$). Each mole of gross CO_2 assimilation produces two moles of PGA. As discussed above, each mole of gross O_2 assimilation produces one mole of PGA directly, and half an additional mole of PGA indirectly when two moles of glycine combine to form one mole of serine, which is eventually reduced to PGA (see Fig. 4.6). The rate of NH_4^+ re-assimilation can be related to the rate of photorespiration as $0.5 v_o$. When taken together, the molar rate of NADPH consumption can be represented as:

$$\text{rate of NADPH consumption} = (2 v_c + 1.5 v_o) + 0.5 v_o \quad (4.11)$$

It is convenient to use an expression relating the rates of carboxylation and oxygenation as follows:

$$\phi = \frac{v_o}{v_c} = \frac{V_{\text{omax}} c_{\text{oc}} K_c}{V_{\text{cmax}} c_{\text{cc}} K_o} = \frac{c_{\text{oc}}}{S_{\text{rel}} c_{\text{cc}}} \quad (4.12)$$

The stoichiometric relations underlying ϕ are illustrated in Figure 4.15. The relations shown in Figure 4.15 are often used in modeling the RPP pathway, as they show how the rates of formation or utilization of all major metabolites in the pathway scale with the rates of Rubisco carboxylation (v_c) and oxygenation (v_o). Using Equation 4.12 for substitution, Equation 4.11 can be simplified to:

$$\text{rate of NADPH consumption} = (2 + 2 \phi) v_c \quad (4.13)$$

The production of each mole of NADPH requires that two moles of electrons move through the photosynthetic electron transport chain. In order to express the rate of NADPH consumption in terms of electron transport rate, the right side of Equation 4.13 must be multiplied by two. Returning now to the fundamental relationship presented in Equation 4.9, the RuBP-limited rate of carboxylation (v_{c2}) ($\mu\text{mol CO}_2 \text{ m}^{-2} \text{ leaf area s}^{-1}$) can be quantitatively expressed as:

$$v_{c2} = \frac{F_J}{4 + 4 \phi} \quad (4.14)$$

where F_J is the rate of photosynthetic electron transport ($\mu\text{mol electrons m}^{-2} \text{ leaf area s}^{-1}$).

4.C.3 Modeling the TPU-limited state

As c_{cc} reaches high values the rate of carboxylation can exceed the rate at which triose-phosphate is converted into sucrose and starch, thus releasing organically-bound P_i . In that condition, P_i can become sequestered in the triose-phosphate pool and the rate of ATP

production can limit the rate of CO₂ assimilation. Limitations by P_i can also occur in some conditions when the utilization of triose-phosphates is constrained by external limitations to plant growth; that is when the rate at which triose phosphates are utilized for new plant growth is lower than the rate of triose phosphate production through photosynthesis. Theoretically, the rate of triose-phosphate utilization will have to occur at one-third the rate of RuBP carboxylation plus one-half the rate of RuBP oxygenation in order to maintain chloroplast P_i balance (Sharkey 1985, Harley et al. 1992b). Thus:

$$v_{c3} = 3 \text{ TPU} + \frac{v_o}{2} \quad (4.15)$$

where v_{c3} is the rate carboxylation ($\mu\text{mol CO}_2 \text{ m}^{-2} \text{ leaf area s}^{-1}$) in the face of P_i limitation and TPU is the rate of triose phosphate utilization ($\mu\text{mol triose phosphate m}^{-2} \text{ leaf area s}^{-1}$). The inclusion of $v_o/2$ on the right side of Equation 4.15 can be understood if it is remembered that for every two moles of phosphoglycolate produced by oxygenation, one mole of PGA is returned to the chloroplast by photorespiration (Fig. 4.7). Thus, photorespiration has the potential to return one P_i equivalent to the RPP pathway for every two oxygenations (see Harley and Sharkey 1991). It is relatively rare to observe v_{c3} as the primary limitation to the rate of carboxylation. As is evident in Figure 4.14, v_{c3} doesn't become a primary limitation to the overall CO₂ assimilation rate until relatively high chloroplast CO₂ concentrations. However, when plants are grown or measured at elevated atmospheric CO₂ concentrations, v_{c3} can emerge as an important control over the rate of CO₂ assimilation (Harley et al. 1992b).

With v_{c1} , v_{c2} and v_{c3} now defined, we can return to the response of CO₂ assimilation rate to c_{cc} and PPF as described by the greater of three possible constraints (Fig. 4.14). At low c_{cc} the availability of CO₂ and kinetic characteristics of Rubisco are considered the primary constraint and carboxylation rate is assumed to be solely limited by v_{c1} . As c_{cc} increases, Rubisco is progressively more limited by RuBP availability, and carboxylation rate is eventually assumed to become solely limited by v_{c2} . Finally, at high c_{cc} , the rate of carboxylation exceeds the rate of P_i recycling, and the carboxylation rate is assumed to be limited solely by v_{c3} . Similar constraints can be applied to the case for low versus high PPF, though v_{c1} limits carboxylation rate at high PPF, v_{c2} limits the rate at low PPF, and v_{c3} probably does not have a limiting role.

4.C.4 Building model links from chloroplast biochemistry to observations on leaves

The equations described to this point are founded on the biochemical processes of the chloroplast. It is difficult to derive quantitative, initial values for each of the parameters of the model (a process called *parameterization*) from biochemical properties alone. A set of additional mathematical relationships has been developed to permit linkage of biochemical processes to leaf-level processes. There are numerous assumptions that must be accepted in order to legitimately make the jump from biochemistry to an intact leaf. The fundamental drivers of photosynthetic biochemistry (i.e., PPFD, [CO₂] and [O₂]) exhibit gradients and transport resistances in the intact leaf that can complicate the matter. Additionally, multiple processes and factors (e.g., metabolite and co-factor concentrations, pH and enzyme turnover), which are controlled at constant and non-limiting levels during *in vitro* assays of biochemical processes, can exert quite different limitations on metabolic fluxes in the intact leaf. All of these complications and uncertainties make the transition from biochemistry to leaves difficult. Nonetheless, there are several 'checks' and 'balances' that can be evaluated in making the transition and to a large degree the scientific community has accepted the validity of chloroplast-to-leaf scaling (see Long and Bernacchi 2003, Sharkey et al. 2007).

Two leaf-level analyses that hold a wealth of biochemical insight are the relations between net CO₂ assimilation rate (A) and PPFD (the so-called A:PPFD curve), and between A and the intercellular CO₂ concentration (c_{ci}) (the so-called A:c_{ci} curve). Intercellular CO₂ concentration refers to the CO₂ concentration within the leaf tissue; in the air spaces contained within the leaf. Intercellular CO₂ concentration is determined by the balance between the biochemical demand for CO₂ by photosynthetic leaf cells and the diffusive supply of CO₂ from the ambient atmosphere, which in turn is regulated by the leaf boundary layer and stomatal conductances (discussed in Chapter 8). The c_{ci} value is calculated from measurements obtained with a leaf gas-exchange system (von Caemmerer and Farquhar 1981).

One of the most important parameters to emerge from A:c_{ci} curves is the CO₂ compensation point. In general terms, the CO₂ compensation point represents the c_{ci} that allows the *gross* rate of photosynthetic CO₂ uptake to be perfectly balanced by the rate of respiratory CO₂ loss. Thus, as c_{ci} is decreased from the value that exists with ambient atmospheric CO₂ concentration, and the gross flux of CO₂ into the leaf also decreases, there will come a point

where the CO₂ flux into the leaf is perfectly balanced by the CO₂ flux out of the leaf. The *net* rate of CO₂ flux (A) at this point is zero and the c_{ci} that exists at this point is referred to as the CO₂ compensation point. There are two types of CO₂ compensation points. The value denoted as Γ is the CO₂ compensation point in the presence of CO₂ efflux from both tricarboxylic acid (TCA) cycle respiration and photorespiration. (TCA cycle respiration occurs in the mitochondria of cells and is involved in cellular energy transformations; it is discussed further in Section 4.D, below.) The value denoted as Γ_* is the CO₂ compensation point in the presence of CO₂ efflux from only photorespiration; this is often called the *photocompensation point*. It is important to recognize how the differences between Γ and Γ_* are reflected in their responses to CO₂ and PPFD, the two principal drivers of A.

Let's consider the responses of Γ and Γ_* to changes in PPFD within the range that limits carboxylation by RuBP availability (i.e., region of v_{c2} limitation). As PPFD increases in the face of limitation by v_{c2}, CO₂ assimilation rate will increase but TCA-cycle respiration will not. In the case of a hypothetical leaf that exists at Γ , an increase in PPFD would require a decrease c_{ci} in order to reduce A and re-establish Γ . In other words, an increase in PPFD will cause a decrease in Γ . This will not be the case for Γ_* . An increase in PPFD, and thus an increase in the rate of RuBP regeneration, will cause proportional increases in the rates of carboxylation and oxygenation at any given c_{ci}. Thus, the c_{ci} that defines Γ_* will remain constant in the face of changing PPFD. The difference between Γ and Γ_* in this regard can be used to measure Γ_* using a combination of A:c_{ci} curves obtained at different PPFD levels (Fig. 4.16). At Γ_* , the assimilation of one molecule of CO₂ through carboxylation is balanced by the loss of one molecule of CO₂ through two oxygenations (i.e., $\phi = 2$). An expression for Γ_* can be derived by recognizing that Γ_* is the value of c_{cc} when $\phi = 2$. Thus:

$$\Gamma_* = \phi \frac{c_{cc}}{2} = \frac{0.5 V_{\text{omax}} K_c c_{oc}}{V_{\text{cmax}} K_o} = \frac{0.5 c_{oc}}{S_{\text{rel}}} \quad (4.16)$$

where Γ_* carries units of mole fraction ($\mu\text{mol CO}_2 \text{ mol}^{-1} \text{ air}$). For the purposes of linking Γ_* to leaf-level gas-exchange measurements, it is assumed that c_{cc} = c_{ci}, an assumption that carries some error, as will be discussed shortly.

Using Γ^* and measured A: c_{ci} curves we can derive $V_{c_{max}}$ according to:

$$\frac{dA}{dc_{ci}} = \frac{V_{c_{max}}}{\Gamma^* + K_c(1 + c_{oc}/K_o)} \quad (4.17)$$

The relationship dA/dc_{ci} is determined as the initial slope of the A: c_{ci} curve, Γ^* is measured in a separate analysis, c_{oc} is taken as the ambient O_2 concentration, and the constants K_c and K_o are taken from past biochemical studies of Rubisco (see Table 2.1).⁴ Equation 4.17 is then rearranged to solve for $V_{c_{max}}$. From its formal derivation, Equation 4.17 is only valid when $c_{ci} \approx \Gamma^*$. It should also be recognized that in this case, $V_{c_{max}}$ reflects the maximum carboxylation rate per unit leaf area, not per unit of enzyme protein. This definition of $V_{c_{max}}$ is apparent in the fact that dA/dc_{ci} is highly correlated with the extracted, maximum activity of RuBP carboxylase obtained from the same leaves (Fig. 4.17).

Using the derived value for $V_{c_{max}}$, and Equation 4.8, the rate of CO_2 assimilation when constrained by Rubisco kinetics (v_{cl}) can be determined within the context of a leaf as:

$$v_{cl} = \frac{V_{C_{max}} c_{ci}}{c_{ci} + K_c (1 + c_{oi}/K_o)} \quad (4.18)$$

Note that in using this relationship the relevant CO_2 and O_2 concentrations are those in the intercellular air spaces of the leaf (c_{ci} and c_{oi} , respectively); these are the values most easily determined from leaf gas-exchange measurements. The most relevant values with regard to Rubisco carboxylation, however, are those in the chloroplast (c_{cc} and c_{oc} , respectively). In the case of O_2 , the difference between c_{oi} and c_{oc} is so small compared to the absolute concentrations, and has such a small effect on the solution to Equation 4.18, that there is no significant error in using c_{oi} . In the case of CO_2 , however, the use of c_{ci} is a simplification that carries some degree of error. The assumption that $c_{ci} = c_{cc}$ ignores resistance to CO_2 diffusion between the intercellular air spaces and the chloroplast stroma. The existence of an internal diffusion resistance is evident in observations of intact leaves using a combination of techniques, including leaf gas-exchange, instantaneous carbon isotope discrimination and chlorophyll fluorescence (Warren 2006). The fact that c_{cc} is lower than c_{ci} means that estimates of A using

Equation 4.18 will be erroneously high when using c_{ci} . Studies using a broad range of species have shown that the presence of this resistance can cause c_{cc} to be as much as 30% lower than c_{ci} (Evans and von Caemmerer, 1996).

Γ_* can also be used to derive an expression for the RuBP-limited rate of carboxylation (v_{c2}). Relying on the simplified assumption that $c_{cc} = c_{ci}$, and using Equation 4.16 to derive a combined expression for Γ_* and ϕ , we obtain:

$$\phi = 2 \Gamma_* / c_{ci} \quad (4.19)$$

Using Equation 4.14 as a starting point, and substituting from Equation 4.19, v_{c2} can now be expressed in terms of Γ_* :

$$v_{c2} = \frac{F_J c_{ci}}{4 c_{ci} + 8 \Gamma_*} \quad (4.20)$$

The whole-chain electron transport rate (F_J) is one of the more poorly-understood components in the current generation of photosynthesis models. In the original version of the Farquhar-von Caemmerer-Berry model (Farquhar et al. 1980b), F_J was entered as an empirical function derived from *in vitro* studies on isolated chloroplasts. The situation has not improved much in the subsequent decades, and we are still left without an electron-transport rate equation derived from the first principles of biochemistry. In light of these deficiencies, F_J continues to be modeled as an empirically-derived, quadratic function, which often takes a form similar to:

$$F_J = \frac{I_2 + F_{J_{\max}} - \sqrt{(I_2 + F_{J_{\max}})^2 - 4 \Theta I_2 F_{J_{\max}}}}{2 \Theta} \quad (4.21)$$

where I_2 is the maximum (potential) photon flux density (moles photons m^{-2} leaf area s^{-1}) that could be used to drive whole-chain electron transport, $F_{J_{\max}}$ is the maximum possible electron transport rate (moles electrons m^{-2} leaf area s^{-1}), and Θ is a unitless curvature factor intended to

'tune' the function with a smooth transition between the PPFD-limited and PPFD-saturated parts of the curve. I_2 is defined as:

$$I_2 = I \cdot a_L \cdot \phi_{\text{PSII, max}} \cdot \beta \quad (4.22)$$

where I is the PPFD incident on the upper surface of the leaf (moles photons m^{-2} leaf area s^{-1}), a_L is the fractional absorptance of the leaf, $\phi_{\text{PSII, max}}$ is the maximum fractional quantum yield for whole-chain electron transport (i.e., the molar ratio of electron transport rate to absorbed photon flux density), and β is the fraction of absorbed light that reaches PSII light harvesting complexes (assumed to be 0.5, Ögren and Evans 1993). The values for I , a_L , and $\phi_{\text{PSII, max}}$ can be measured. The values for F_{Jmax} and Θ are typically determined from empirical fitting of the A:PPFD response curve (see Bernacchi et al. 2003).

It should be noted that Equation 4.20 has been derived to reflect the requirement for four electrons to be transported through the electron transport chain to reduce ferredoxin and produce two reduced NADPH molecules which then drive the assimilation of one CO_2 molecule. Alternative forms of the model have been published that assume ATP as the primary limitation to RuBP regeneration (Long 1991, Bernacchi et al. 2003), or a combination of ATP and NADPH (Yin et al. 2004), with the principal difference being slight adjustments to the denominator of Equation 4.20.

The influence of temperature on A is modeled through a derivation of the Arrhenius equation (see Section 3.A). The temperature dependencies of variables such as ϕ , Γ^* , and α_c are ultimately determined by the temperature dependencies of K_c , K_o , V_{cmax} , V_{omax} according to:

$$\text{Parameter } (K_c, K_o, V_{\text{cmax}}, V_{\text{omax}}) = \exp^{(c-Ea/RT)} \quad (4.23)$$

where c is a scaling constant. Equation 4.23 carries the condition that the target parameter increases continuously with temperature. In those cases where a parameter exhibits a high temperature threshold and decreases at higher temperatures (e.g., due to enzyme denaturation) the temperature dependencies are modeled with a modified version of Equation 4.23 in which

entropy and energy of deactivation terms are added. In past models, this has been done for example with the V_{cmax} and V_{omax} terms (Harley et al. 1992b, Bernacchi et al. 2001).

Using the models of v_{c1} , v_{c2} and v_{c3} that were described above, it is now possible to model net CO₂ assimilation rate (A) in an intact leaf. Under any set of defined environmental conditions, A is assumed to equal the minimum of v_{c1} , v_{c2} , or v_{c3} minus the rates of photorespiratory and non-photorespiratory CO₂ loss:

$$A = \min \{ v_{c1}, v_{c2}, v_{c3} \} - 0.5 v_o - R_d \quad (4.24)$$

where R_d is the rate of tricarboxylic acid cycle CO₂ loss (or 'dark' respiration), all fluxes carry units of $\mu\text{mol CO}_2 \text{ m}^{-2} \text{ leaf area s}^{-1}$, and $\min \{ \}$ represents the 'minimum of'.

Recognizing that $v_o = v_c \phi$, and that ϕ can be related to Γ_* according to Equation 4.19, we can rewrite Equation 4.24 as:

$$A = (1 - \Gamma_*/c_{ci}) \min \{ v_{c1}, v_{c2}, v_{c3} \} - R_d \quad (4.25)$$

When modeled according to these relationships, one obtains response curves similar to those shown in Figure 4.14, with a prominent feature being a sharp transition between the regions limited by v_{c1} , v_{c2} , and v_{c3} . The sharp transition is an artifact created by the structure of the model as the minimum of three processes. In a real leaf individual chloroplasts will differ in the degree to which v_{c1} , v_{c2} or v_{c3} limit A at any instant in time, and they will face intra-leaf gradients in PPFD and CO₂, all of which will blend, or smooth, the response of the leaf-averaged A to PPFD and CO₂. The transitions are often 'softened' in the model through quadratic 'tuning' using the following relationship:

$$\theta A^2 - A (v_{c1} + v_{c2}) + (v_{c1} v_{c2}) = 0 \quad (4.26)$$

where θ is a convexity factor. As $\theta \rightarrow 0$, the modeled response of A to PPFD or c_{ci} will exhibit a non-rectangular hyperbola. As $\theta \rightarrow 1$, the response will exhibit a sharp transition. The presence

of θ in Equation 4.26 can be thought of as calibrating the degree to which v_{c1} and v_{c2} combine to influence the shape of the transition. Similar 'tuning' can be applied to transitions involving v_{c3} .

Many of the parameter values required to run the model of A in C_3 plants are presented in Table 3.1. Some of these exhibit little variation across a range of different C_3 species. For variables such as the K_c and K_o for Rubisco, which exhibit less interspecific variation, a single value can be used in parameterizing the model for different C_3 species. Variables such as c_{ci} and Γ^* are also somewhat conserved among different C_3 species. The variable V_{cmax} is related to the allocation pattern of N, a growth-limiting resource, and is thus strongly dependent on plant growth form. The mechanisms that control the allocation of nitrogen to V_{cmax} in different plant growth forms are not well understood. As a result, V_{cmax} is typically prescribed based on its tendency to fall within certain bounds for various plant growth forms, or it is determined empirically from the carboxylation efficiency using Equation 4.17.

Also problematic is our limited ability to predict dynamics in V_{cmax} and R_d in the face of ontogenetic change and longer-term environmental stresses such as occur during drought or periods of extreme temperature. One of the complicating aspects of these responses is that they depend on stochastic features of the environment, such as how quickly stress occurs. Dynamics in model parameters due to these influences are currently represented by empirically-derived relationships. Recently, breakthroughs have been made in our understanding of the longer-term effects of elevated atmospheric CO_2 concentration on photosynthetic biochemistry and control over CO_2 assimilation rate (Box 4.1). This has provided the promise that we will soon be able to derive fundamental, biochemically-based models of the response of plants to a changing atmosphere.

To this point, we have considered plants that solely possess the C_3 photosynthetic pathway. Plants of this photosynthetic type account for most of the terrestrial plant biomass on the earth. However, plants with the C_4 photosynthetic pathway are also significant in key ecosystems, such as tropical and subtropical grasslands, that exert strong influences on global budgets for CO_2 and H_2O (Collatz et al. 1998, Still et al. 2003). The C_4 photosynthetic pathway has evolved in the angiosperms (flowering plants) in response to historical declines in the atmospheric CO_2 concentration and increase in the atmospheric O_2 concentration, both of which promote high photorespiration rates in low latitude ecosystems with frequent warm temperatures (Box 4.2).

The C₄ pathway has evolved at least 50 times independently, a fact which by itself suggests that the selective pressures of enhanced photorespiration rates have had a significant negative influence on plant fitness in certain environments (Sage 2004, Monson and Collatz 2009).

4.D Tricarboxylic acid cycle respiration ('dark respiration')

'Dark respiration' (R_d) refers to non-photorespiratory mitochondrial respiration in plant tissues which, despite the name, occurs in both the dark and light. As our focus is on plant-atmosphere interactions, we will be most concerned with the fluxes of CO₂ and O₂ that originate from dark respiration. Other perspectives that we will *not* cover include the energetics of respiration and the respiratory costs of specific cellular processes. Respiratory CO₂ is derived from the enzymatic oxidation of carbon substrate by pyruvate dehydrogenase, a large mitochondrial protein complex that links the glycolytic metabolic pathway to the tricarboxylic acid (TCA) pathway (also called the Krebs cycle), and two enzymatically-catalyzed steps in the TCA pathway itself (Fig. 4.18). There are a number of more minor pathways that also emit CO₂ (e.g., the synthesis of tyrosine and phenylalanine in the chloroplast), but the primary flux from plants is from the mitochondrial processes. Several possible substrates can be utilized by enzymes in the TCA cycle, including carbohydrates, proteins, and fatty acids. We will focus on carbohydrates; the most frequently used respiratory substrates in leaves.

Terrestrial plant R_d represents a large flux of CO₂, both in terms of absolute magnitude and as a fraction of photosynthesis. In a survey of past literature, Amthor (2000) concluded that R_d represents 30-50% of gross photosynthesis minus photorespiration [i.e., $v_c (1 - \Gamma_*/c_{ci})$] in crop ecosystems and 50-75% in natural ecosystems. The amount of CO₂ lost through R_d is dependent on plant size, the ratio of photosynthetic to non-photosynthetic biomass, growth rate, and recent environmental history. Large, actively growing plants, with a high proportion of non-photosynthetic, but metabolically-active biomass (e.g., stems and roots), growing in warm climates will exhibit the highest respiration rates. The highest respiration-to-photosynthesis ratios are found in saline ecosystems where plants maintain high rates of ATP-driven ion transport. The rate of R_d is influenced by the amount of photosynthetic substrate available to the plant and the temperature of the environment. Thus, it is likely that future changes in atmospheric CO₂ concentration and climate will cause changes to the respiratory CO₂ flux from terrestrial ecosystems (Gifford 2003, Gonzelez-Meller et al. 2004, Luo 2007).

4.D.1 Models of R_d

Considerable progress has been made in understanding the biochemical controls over the flux of carbon through the steps of glycolysis and the TCA cycle (Plaxton 1996, McIntosh et al. 1998, Tovar-Mendez et al. 2003). The derivation of an integrated, mechanistic model of R_d , however, has proven problematic (Ferne et al. 2004). The primary obstacle involves coupling the loss of CO_2 and heat to the energetic demands of cellular maintenance and growth (e.g., the energy required for ion transport, protein turnover, membrane repair, or cell wall construction) (see Cannell and Thornley 2000, Thornley and Cannell 2000). Such coupling requires knowledge about substrate-use efficiency, cellular enthalpy and carbon channeling to growth versus maintenance, which does not yet exist.

In the absence of generalized knowledge about the mechanisms linking cellular energetics to CO_2 loss, R_d has been modeled as a scaled function of either, the rate of photosynthate utilization, the rate of net photosynthesis, or the general effect of temperature on the rate of metabolism. The first approach has proven most useful in modeling respiration within the context of plant growth, and longer-term plant carbon budgets. The second and third approaches have proven most useful in modeling the instantaneous rate of respiration and its response to short-term changes in the environment.

The empirical basis for scaling R_d to the rate of photosynthate utilization was originally provided by McCree (1970) for whole plants, and the theoretical basis was developed by Thornley (1970, 1971). In both sets of studies it was reasoned that at steady state all of the sugar phosphates produced from photosynthesis would (1) be converted to respired CO_2 as they are utilized in the production of energy for cellular maintenance, (2) be converted to respired CO_2 as they are used to produce energy for cellular growth, or (3) be converted to various carbon substrates that support new growth. This logic is expressed in formal terms as:

$$\Delta S = \Delta S_m + \Delta S_{gr} + \Delta S_{gb} \quad (4.27)$$

where ΔS represents the total respiratory substrate used during a specified time period (Δt), ΔS_m represents the substrate respired as CO_2 during the production of energy for cellular maintenance (often called *maintenance respiration*), ΔS_{gr} represents the substrate respired as CO_2 during the

production of energy to support new growth (often called *growth respiration*), and ΔS_{gb} is the substrate that is used to produce new biomass; all expressed in units of moles. In terms of estimating the respiratory CO₂ yield, only S_m and S_{gr} are relevant. Using Equation 4.27 as a foundation:

$$R_d = 6 (\Delta S_m + \Delta S_{gr}) / W \Delta t \quad (4.28)$$

where R_d represents the average dark respiration rate (mol CO₂ g⁻¹ biomass s⁻¹), the factor 6 represents the molar equivalent of CO₂ produced from the carbohydrate substrate (in this case glucose equivalents) used in $\Delta S_m + \Delta S_{gr}$, W is biomass (g), and Δt is a finite time interval (s).⁵ The McCree/Thornley model was derived for whole plants (which accommodated the respiratory use of photosynthate that is exported from photosynthetic leaf cells to the roots, stems and growing apices) and for time intervals on the order of a day (which accommodated the oxidation of stored photosynthate during the night).

Although Equation 4.28 provides a theoretical basis for understanding the components of R_d , it is largely intractable for prediction of the instantaneous respiration rate; which would be most useful for inclusion with models of photosynthesis. In order to move the modeling toward the instantaneous time step, the growth and maintenance concepts reflected in Equation 4.28 can be related to instantaneous flux coefficients as:

$$R_d = R_{gr} + R_m = (g_R G + m_R W) / W \quad (4.29)$$

where R_{gr} and R_m are the growth and maintenance respiration rates (mol CO₂ g⁻¹ existing biomass s⁻¹), respectively, G is the growth rate (g new biomass s⁻¹), W is existing biomass (g), and g_R and m_R are scaling coefficients with units mol CO₂ g⁻¹ new biomass and mol CO₂ g⁻¹ existing biomass s⁻¹, for growth respiration and maintenance respiration, respectively.

Experimental approaches to measure g_R and m_R have included (1) component partitioning, in which the theoretical energetic costs of individual metabolic processes are summed to provide composite CO₂ fluxes, and (2) regression analyses, in which R_d is regressed against W in leaves or plants that are no longer growing [thus assuming that the term $(g_R G) \rightarrow 0$] to derive a value for m_R (see Amthor 2000). These approaches have not been entirely satisfactory as gaps in our

knowledge cause the first approach to suffer from undefined (and therefore missing) metabolic components, and the second approach relies on non-validated assumptions about the constancy of maintenance costs as a function of tissue age.

In some past models g_R has been related to 'growth efficiency' using an analog originally developed for microbial growth and respiration. The rate of CO₂ production (R) by a growing population of microorganisms can be defined as:

$$R = \frac{(1 - Y_g)}{Y_g} \mu_M X_{(t_0)} \quad (4.30)$$

where R has units of mol CO₂ s⁻¹, Y_g is the growth yield (the fraction of carbon substrate that is converted to microbial biomass, and thus is not available for respiratory CO₂ loss), μ_M is the rate at which substrate carbon is used for microbial growth (mol substrate C g⁻¹ biomass s⁻¹), and $W_{(t_0)}$ is the microbial biomass (g) at time 0. Thus, R reflects the residual carbon available for respiration after accounting for the carbon demands of biomass increase. Thornley (1970) developed an analog for plants, which, when expressed to provide biomass specific respiration, can be written as:

$$R_d = \frac{(1 - Y_g/Y_g)G + m_R W}{W} \quad (4.31)$$

Equation 4.31 can be related to Equation 4.29 by recognizing that $Y_g = 1/(1+g_R)$. Equation 4.31 provides a context within which to explore tradeoffs between growth efficiency and respiration. On a molar basis, an increase in the efficiency of carbon-substrate utilization for increase in biomass must occur with a decrease in the amount of CO₂ lost from the growth process. Equation 4.31 doesn't easily solve the issue of tractability, however, since we are now faced with a different unknown coefficient, Y_g , that must be defined.

More recently, some workers have argued that the theoretical foundation for coupling respiration to growth is best developed through a complete thermodynamic framework that takes account of not only the conservation of mass and chemical energy, but also heat (e.g., Macfarlane et al. 2002). The enthalpy-balance model (Hansen et al. 1994) is written as:

$$\begin{array}{cccc}
 R_{SG} \Delta H_B & = & - R_d \Delta H_{CO_2} & - q & (4.32) \\
 \text{Term I} & & \text{II} & \text{III} &
 \end{array}$$

where R_{SG} is the biomass-specific rate of conversion of substrate into biomass ($\text{mol C g}^{-1} \text{ biomass s}^{-1}$), ΔH_B is the change in enthalpy when a mole of substrate C is converted into biomass C ($\text{kJ mol}^{-1} \text{ C}$), R_d is the rate of respiratory CO_2 production ($\text{mol CO}_2 \text{ g}^{-1} \text{ biomass s}^{-1}$), ΔH_{CO_2} is the change in enthalpy for the conversion of substrate C to CO_2 ($\text{kJ mol}^{-1} \text{ C}$), and q is the metabolic heat rate ($\text{kJ g}^{-1} \text{ biomass s}^{-1}$). Equation 4.32 balances the total change in enthalpy channeled into the conversion of substrate to biomass (Term I) against the loss of enthalpy due to respiratory oxidation of substrate to CO_2 (Term II) and the loss of heat (Term III). The equation can be rearranged to solve for R_d . By convention, the negative signs on the right-hand side of the equation reflect exothermic processes. The terms in Equation 4.32 are resolved through a combination of chemical composition analyses, calorimetric combustion and measurement of respiratory energy-efficiency quotients. The advantage to using Equation 4.32 is that it places respiratory flux into a thermodynamic context capable of accommodating different enthalpy conversion efficiencies among diverse processes (e.g., O_2 -dependent respiration versus cyanide-resistant respiration) and is thus better able to couple R_d to the energetic demands of growth and tissue maintenance.

None of the modeling approaches described to this point provides a direct linkage to photosynthetic carbon assimilation that would permit representation of R_d in photosynthesis models. In order to accommodate such linkage, researchers have often rejected formal models of R_d , and instead, they have represented R_d through linear scaling with $V_{C_{max}}$. Past studies have revealed that R_d measured on mature foliar tissues for a number of plant species is linearly related to N concentration (Fig. 4.19). This relationship is not unexpected given that up to 60% of maintenance respiration can be devoted to supporting protein turnover (Penning de Vries 1975), and proteins are the primary biological sink for foliar N. Similar linear dependencies have been observed for $V_{C_{max}}$ and $F_{J_{max}}$ (when regressed against leaf N concentration) (Fig. 4.20), providing good biochemical justification for the linear scaling of R_d with $V_{C_{max}}$. There are caveats that must be considered in applying these simple scaling relationships. For example, in those species (e.g., conifers) in which a significant fraction of foliar N occurs in storage or

structural compounds, rather than enzymes, the positive correlation between R_d and $[N]$ may still be present, but muted and difficult to detect (Kruse and Adams 2008). Nonetheless, in past studies that combine measurements of net CO_2 assimilation rate (A) and R_d , it has been shown that these two variables are linearly correlated across a broad range of species (Gifford 1994, Ceulemans and Saugier 1991, Ryan et al. 1994). Furthermore, Collatz et al. (1991) and Amthor (1994) showed that photosynthetic models parameterized with the linear constant $R_d/V_{C_{max}} = 0.015$ are well-validated with observations of leaf gas exchange.

One of the tools that have proven useful to integrating carbon flows through both photosynthesis and respiration is stable isotope analysis. As carbon flows serially from the atmosphere, through the photosynthetic and respiratory processes of the leaf, and back to the atmosphere, the ^{13}C and ^{12}C isotopes are exposed to differential fractionation at several steps. Analysis of those fractionations has provided valuable insight into the controlling steps over carbon flow and allocation at the cellular scale (see Box 4.3).

4.D.2 The temperature dependence of R_d

In fully-expanded leaves, the CO_2 efflux due to growth respiration will be minimal; in such leaves, $R_d \approx R_m$. In cellular terms, R_m is the CO_2 cost of providing energy for protein synthesis, ion transport, and repair of cellular constituents. Maintenance respiration rate is highly sensitive to temperature. On theoretical grounds, the temperature dependence of R_m should follow the same Arrhenius relationships that hold true for other chemical reactions; i.e., the temperature-dependent rate constant should be defined as $k = C e^{-E_a/RT}$ (see Section 3.A). By convention, however, a slightly different relation has come to be favored in the biological sciences; i.e., $k = A e^{BT}$, where A and B are empirically-determined scaling coefficients. This relation was first described by van't Hoff in 1898, approximately 10 years after Arrhenius' original work was published, and has emerged as the most commonly-used temperature-dependence model in the biological sciences, the so-called *Q₁₀ model* (see Appendix 3.1 for a formal derivation of the Q_{10} relation). In applying the Q_{10} relation to a respiration model, we can write:

$$R_m = R_0 e^{(\ln Q_{10}/10)\Delta T} \quad (4.33)$$

where R_0 is the respiration rate at a standard temperature and ΔT is the temperature difference between the standard temperature and the new temperature. As an example of application of the Q_{10} model, if R_m doubles in response to a 10°C increase in temperature, then the Q_{10} is 2.

For most plants the Q_{10} for respiration rate ranges between 1.5 and 3.0; a value of 2.0 is often used as "typical" for plant tissues. However, the Q_{10} varies with temperature, and values near 2.0 are only found over a narrow temperature range ($20\text{-}30^\circ\text{C}$). Over a broader range, the Q_{10} decreases with increasing temperature, from values near 3.0 at temperatures less than 10°C to values near 1.5 at temperatures greater than 35°C (Atkin and Tjoelker 2003). The decrease in Q_{10} with increasing temperature is, at least in part, due to shifts in the Boltzmann distribution of reactant kinetic energy as temperature increases (see Section 3.A). As temperature increases, the fraction of molecules with kinetic energy exceeding the energy of activation (E_a) increases; but, it increases more in a lower range of temperatures than in a higher range of temperatures. Other factors may also be involved in the temperature dependence of Q_{10} , including shifts in the limitations imposed by enzyme activity versus substrate availability and changes in the fluidity of the mitochondrial membranes in which respiratory proteins are embedded and across which respiratory metabolites are transported (Sharpe and De Michelle 1977, Hoefnagel et al. 1998). Fortunately for modeling efforts, the temperature dependence of the Q_{10} is linear across the biologically-relevant temperature range from $10\text{--}40^\circ\text{C}$, and highly conserved across a broad range of plant species (Atkin and Tjoelker 2003). In this case, the temperature dependence of the Q_{10} refers to short-term (e.g., hours) changes in temperature.

In addition to dependence on short-term dynamics in temperature (seconds-to-minutes), R_d is also dependent on longer-term temperature history (hours-to-days). Thus, a process known as *temperature acclimation* occurs in the respiratory properties of plants. The temperature dependence of R_d can exhibit a higher or lower thermal optimum when plants have experienced higher or lower temperatures in their recent past, respectively (Atkin et al. 2005). The potential for respiratory acclimation varies among species, and general trends on which predictions can be based have been difficult to derive. The exact causes of the acclimation are still not fully resolved, although it is known that newly emerged leaves have greater potential to adjust to a new temperature regime than fully-expanded leaves (Ow et al. 2008) and that acclimation in both R_d and A facilitates a nearly constant ratio of the two CO_2 fluxes within the temperature range

normally encountered by a plant. (An increase in the ratio of $R_d:A$ can occur when plants acclimate to temperatures that exceed their normal range; Atkin et al. 2005, 2007).

4.E Volatile Organic Compounds

Plants not only exchange inorganic C (e.g., CO_2) with the atmosphere, but also a broad range of organic C in the form of volatile organic compounds (VOCs). The magnitude of the global VOC flux is small compared to the magnitude of photosynthetic and respiratory CO_2 fluxes; approximately 2 Pg of VOCs emitted annually compared to approximately 120 Pg of CO_2 exchanged annually through gross photosynthesis and terrestrial respiration, respectively. However, the VOC flux is important for understanding the gas-phase reactions of atmospheric chemistry, as well as the production of atmospheric aerosol particles which influence the earth's radiation budget (Fehsenfeld et al. 1992, Fuentes et al. 2000, Monson and Holland 2001, Monson 2009). Went (1960) first described the importance of plants as sources for VOCs when he used the concentration of terpene-containing leaf oils in sagebrush plants to estimate global terpene emissions as 175 Tg C y^{-1} . Since that seminal study, estimates of global emissions have been refined through the use of coupled global atmospheric chemistry and transport models, and are now estimated to be $2,400 \text{ Tg C y}^{-1}$ (Guenther 2002). A broad range of organic compounds are emitted from plants (see Kesselmeier and Staudt 1999, Monson 2002). One of the principal types of emitted VOCs is the *terpenes*. Terpenes have long-chain, carbon backbones with the most common forms ranging from 5-15 carbons in length, and with one or more C-C double bonds; thus, characterizing them as organic *alkenes*. The presence of double bonds in the carbon skeleton provides an electron source that is attacked by atmospheric oxidants, such as hydroxyl radicals ($\text{OH}\cdot$), nitrate radicals ($\text{NO}_3\cdot$) and ozone (O_3), thus initiating an active sequence of photochemical reactions. The most common terpenes emitted from plants include: isoprene (C_5H_8), monoterpenes ($\text{C}_{10}\text{H}_{16}$), and sesquiterpenes ($\text{C}_{15}\text{H}_{24}$). These compounds are produced for a variety of purposes, including protection from oxidative and thermal stresses in the chloroplast, protection from herbivory, and possibly the maintenance of metabolic homeostasis (Harley et al. 1999, Sharkey and Yeh 2001, Monson et al. 2007).

In terms of atmospheric chemistry, the most important terpene emitted from plants is, arguably, *isoprene* (2-methyl-1,3-butadiene), which has five carbon atoms per molecule. Global

isoprene emissions are likely to be in the range 500-550 Tg C yr⁻¹ (Arneth et al. 2008). Isoprene reacts relatively quickly with OH· radicals in the atmosphere, and only has an atmospheric lifetime of 1-2 hours. The emissions of *monoterpenes* (with ten carbon atoms per molecule) are also important contributors to photochemical reactions in the atmosphere. It is the monoterpenes, and in particular camphor, that compose the leaf oils of sagebrush used in Fritz Went's original estimate of global VOC emissions. Current estimates of global monoterpene emissions are in the range 100-120 Tg yr⁻¹ (Arneth et al. 2008). Like isoprene, monoterpenes are oxidized mostly through reaction with atmospheric OH· radicals. Monoterpene lifetimes are in the range of 3-6 hours, a bit longer than those for isoprene. Most recently, tropical ecosystems have been identified as strong monoterpene sources, with potentially profound effects on regional atmospheric chemistry (Kesselmeier et al. 2002, Kuhn et al. 2004, Karl et al. 2007, Wang et al. 2007). A third important class of plant-emitted terpenes is the *sesquiterpenes* (C₁₅ hydrocarbons). Some of the more commonly-emitted sesquiterpenes (e.g., β-caryophyllene) react so quickly with OH· radicals that they have tropospheric lifetimes of only 1-2 minutes. Sesquiterpenes are thought to be particularly important in controlling the rate of secondary organic aerosol formation in the atmosphere (Sakulyanontvittaya et al. 2008).

In addition to terpenes, a variety of oxygenated VOCs are emitted from plant leaves (see Fall 1999). Acetone is emitted at global rates of approximately 95 Tg yr⁻¹ and an important source is the expanding buds on the shoots of conifer trees. Methanol is emitted from vegetation at the rate of 80-130 Tg yr⁻¹, with an important source being the demethylation of pectin compounds in the expanding cell walls of leaves. Methylbutenol (2-methyl-3-buten-2-ol) is an oxidized hemiterpene, similar in structure and biochemical origin to isoprene, and emitted at relatively high rates from North American pine forests. Estimates of global methylbutenol emissions are not available; however regional estimates for North America suggest emissions of 3.2 Tg C yr⁻¹ (Guenther et al. 2000). Acetaldehyde emissions occur from numerous different types of plants, and may be associated with vegetative stress. Short-chain organic acids, including formic and acetic acids, are emitted from many plants and soil microbes.

4.E.1 Biochemical models of plant VOC emissions

The rate of VOC emission from leaves is best modeled in terms of the instantaneous effects

of temperature, CO₂ and photon flux density on metabolism and compound volatility (in the case of temperature). We don't understand enough about the longer-term controls on VOC production (e.g., in response to water stress, seasonal climate changes, phenology, decadal-scale climate change) to make predictions about the effect of climate variability or changes in the CO₂ concentration of the atmosphere. For the case of isoprene emissions, the rate of synthesis is tightly coupled to instantaneous chloroplast metabolism, including net CO₂ assimilation rate (Fig. 4.21). In fact, the isoprene emitted by leaves is constructed in the chloroplast using carbon substrates produced from recent photosynthesis (Sharkey and Yeh 2001). Using the connection to photosynthesis we have been able to develop good models of the short-term, temperature-, PPFD- and CO₂-dependence. The responses of isoprene emission rate (I_s) to temperature, PPFD and CO₂ can be estimated as:

$$\begin{aligned}
 I_{sT} &= f \left\{ I_{sb}, \exp^{c_1/RT_L} \right\} \\
 I_{sPPFD} &= f \left\{ I_{sb}, \frac{\alpha c_2 I}{\sqrt{1 + \alpha^2 I^2}} \right\} \\
 I_{sCO_2} &= f \left\{ I_{sb}, I_{smax} - \frac{I_{smax} c_{ci} h}{c_3 + c_{ci} h} \right\}
 \end{aligned} \tag{4.34}$$

where each of the equations shows dependence on the basal isoprene emission rate (I_{sb}) which represents the rate of isoprene emission under a standard set of measurement conditions (typically leaf temperature (T_L) = 30 °C, PPFD (I) = 1,000 $\mu\text{mol m}^{-2} \text{s}^{-1}$, and atmospheric CO₂ mole fraction (c_{ca}) = 400 $\mu\text{mol mol}^{-1}$), and c_1 , c_2 and c_3 , and c_4 represent scaling coefficients, I_{smax} represents the maximum isoprene emission rate, α represents the initial slope of the PPFD-dependence curve, I represents incident PPFD, and T represents leaf temperature. The exact forms of the relevant functions that relate I_s as a variable dependent on I_{sb} , and either T_L , I or c_{ci} can be found in the literature (Guenther et al. 1991, 1993, Wilkinson et al. 2009), but they are presented here in general form to show the similarities in isoprene emission modeling and the models derived previously for photosynthetic CO₂ assimilation rate. The temperature dependence of I_s exhibits a form similar to the Arrhenius equation presented above, and presumably reflects the temperature dependence of isoprene synthase, the enzyme that catalyzes the final step in isoprene biosynthesis (Fig. 4.22). The PPFD dependence reflects a rectangular

hyperbola, similar to that developed for photosynthetic electron transport rate; given the dependence of isoprene biosynthesis on the products of photosynthesis, it is not surprising that I_s reflects a similar dependence on PPFD. The one surprising relation, at least with regard to photosynthesis, is the CO_2 response, which shows that I_s will decrease as c_{ci} increases; opposite to the relation between A and c_{ci} . The inhibition of I_s by c_{ci} is presumably due to enzymatic control over processes not directly related to net CO_2 assimilation (see Rosenstiel et al. 2003). The general form of the relationship between $I_{s\text{CO}_2}$ and c_{ci} , as shown in Equation 4.34 is similar to that of the Michaelis-Menten model, which works well for predicting enzyme-substrate interactions. This similarity follows from rational argument if the CO_2 response of isoprene emission is dependent in inverse manner on the activity of a key controlling enzyme.

Our ability to model the emission of monoterpenes and sesquiterpenes is considerably more limited than that for isoprene. Monoterpene emissions from broad-leaved trees tends to be light-dependent and linked to instantaneous metabolism, although it can also be emitted at relatively high rates from stored monoterpenes in surface trichomes. In the case of Mediterranean oak trees, monoterpene emission occurs from the chloroplasts in a manner that is similar to that for isoprene emissions; in that case, we can use the same models described above for isoprene can be used to predict monoterpene emissions. In other cases, for example for monoterpene emissions from many tropical forest trees, we don't yet understand the metabolic controls over the light-dependent monoterpene emissions. Models for those emissions are not yet available. Monoterpene emissions from coniferous trees often occur from stored reservoirs contained in resin blisters or resin canals. In these cases, the emission rate can be modeled on the basis of the vapor pressure of the compound contained in the air of resin canals or surface resin blisters (Lerdau et al. 1997).

4.F NH_3 and NO_2 Metabolism

Human activities, such as agricultural husbandry and biomass burning, cause the emission of NH_3 and NO_2 to the atmosphere (Monson and Holland 2001), creating a reservoir of molecules capable of participating in atmospheric chemistry or being deposited back to the surface, often times through processes involving plants. The assimilation of NH_3 and NO_2 into leaf cells from the atmosphere can occur through the normal metabolic pathways involved in photorespiration and nitrate assimilation, respectively. Plants are also capable of emitting NH_3

and NO_2 . Whether leaves act as sources or sinks for NH_3 and NO_2 , is determined by the concentrations of each compound in the atmosphere relative to the intercellular air spaces of the leaf (Sparks 2009). Thus, we can identify a leaf compensation point for these compounds, similar to the CO_2 compensation point that was discussed above (see Section 4.C.4; Krupa 2003, Sparks et al. 2001, Lerdau et al. 2000). As a general estimate, the intercellular air spaces of a C_3 leaf will contain NH_3 at $\sim 2.5 \text{ nmol mol}^{-1}$ during normal metabolism (e.g., Farquhar et al. 1980a). General measurements of NH_3 concentrations in the atmosphere range from $0.2\text{-}15 \text{ nmol mol}^{-1}$ (Roberts et al. 1988, Krupa 2003). Thus, a broad range of observations exist at which NH_3 would be assimilated by plants, and a relatively narrow range of observations exist at which vegetation would act as a source for NH_3 . In a detailed case study of a montane forest site, which receives air from relatively undeveloped landscapes with NH_3 concentrations of $0.2\text{-}0.3 \text{ nmol mol}^{-1}$, or agriculturally-developed landscapes with NH_3 concentrations of $5\text{-}6 \text{ nmol mol}^{-1}$, Langford and Fehsenfeld (1992) found that the forest vegetation acted alternately as a source or sink for atmospheric NH_3 depending on wind direction; the forest-averaged NH_3 compensation point was $\sim 1 \text{ nmol mol}^{-1}$.

Measurements of NO_2 uptake by isolated leaves have also revealed an apparent compensation point, with most estimates in the range $1\text{-}3 \text{ nmol mol}^{-1}$ (Weber and Rennenberg 1996, Hereid and Monson 2001, Sparks et al. 2001). We might predict that vegetation is a source of NO_2 at sites with atmospheric concentrations below this range, and a sink at sites with concentrations above this range. Measurements of NO_2 exchange above forests, however, have revealed uptake of NO_2 at most atmospheric concentrations, including some as low as $0.2 \text{ nmol mol}^{-1}$ (Jacob and Wofsy 1990, Rondon et al. 1993). This has led some to doubt the validity of the compensation points that have been measured in the past (Lerdau et al. 2000). Most models that are constrained by the need for mass balance in the atmospheric NO_x budget (which includes NO and NO_2) predict that plants should be an NO_2 sink at most places on the globe.

Table 2.1. Approximate parameter values for the C₃ model of CO₂ assimilation rate.*

Parameter	Value range	Description
K_c (from <i>in vitro</i> assay)	250-300 $\mu\text{mol mol}^{-1}$	Michaelis-Menten coefficient for CO ₂ for C ₃ Rubisco
K_c (from <i>in vivo</i> assay)**	405 $\mu\text{mol mol}^{-1}$	Michaelis-Menten coefficient for CO ₂ for C ₃ Rubisco
K_o (from <i>in vitro</i> assay)	400-450 mmol mol^{-1}	Michaelis-Menten coefficient for O ₂ for C ₃ Rubisco
K_o (from <i>in vivo</i> assay)**	278 mmol mol^{-1}	Michaelis-Menten coefficient for O ₂ for C ₃ Rubisco
$V_{C_{\text{max}}}$		Maximum carboxylation rate***
agricultural crops	90-180 $\mu\text{mol CO}_2 \text{ m}^{-2} \text{ s}^{-1}$	
deciduous trees	50 $\mu\text{mol CO}_2 \text{ m}^{-2} \text{ s}^{-1}$	
coniferous trees	25 $\mu\text{mol CO}_2 \text{ m}^{-2} \text{ s}^{-1}$	
tropical trees	50 $\mu\text{mol CO}_2 \text{ m}^{-2} \text{ s}^{-1}$	
understory herbs	70 $\mu\text{mol CO}_2 \text{ m}^{-2} \text{ s}^{-1}$	
desert annuals	150 $\mu\text{mol CO}_2 \text{ m}^{-2} \text{ s}^{-1}$	
sclerophyllous shrubs	50 $\mu\text{mol CO}_2 \text{ m}^{-2} \text{ s}^{-1}$	
$V_{O_{\text{max}}}$	0.25 $V_{C_{\text{max}}}$	Maximum oxygenation rate
TPU	20-60 $\mu\text{mol CO}_2 \text{ m}^{-2} \text{ s}^{-1}$	Triose-phosphate utilization rate
α	0.050 mol CO ₂ mol ⁻¹ photons absorbed	quantum yield for CO ₂ assimilation in normal air
α_c	0.075 mol CO ₂ mol ⁻¹ photons absorbed	CO ₂ -saturated quantum yield for CO ₂ assimilation
Γ^*	35 $\mu\text{mol CO}_2 \text{ mol}^{-1}$	CO ₂ photocompensation point
c_{oc}	210 mmol mol^{-1}	O ₂ concentration in chloroplast
c_{ci}	235-250 $\mu\text{mol CO}_2 \text{ mol}^{-1}$	Intercellular CO ₂ concentration
c_{cc}	210-225 $\mu\text{mol CO}_2 \text{ mol}^{-1}$	CO ₂ concentration in chloroplast
R_d	0.015 $V_{C_{\text{max}}}$	Whole-leaf respiration rate

* All values are estimated for 25°C

** Determined from analysis of a Rubisco-antisense line of tobacco with reduced *in vivo* Rubisco concentrations.
From: Bernacchi et al. (2001)

*** Values for $V_{C_{\text{max}}}$ for C₃ plants were taken from Wullschlegel (1993)

Appendix 4.1 Derivation of the summation and connectivity theorems

Of all the various components of Metabolic Control Analysis, the summation theorem most reflects the fundamental tenet of 'shared' control over metabolic flux. In order to derive the summation theorem, we state the assumption that enzyme activity is proportional to enzyme concentration, and the recognition that in the face of perturbation to the concentration of a single enzyme, the change in flux through a pathway will be affected as follows:

$$dF = \frac{\partial F}{\partial c_{E1}} dc_{E1} + \frac{\partial F}{\partial c_{E2}} dc_{E2} + \frac{\partial F}{\partial c_{E3}} dc_{E3} + \dots \quad (4.35)$$

Dividing Equation 4.35 by F to express all derivatives on a fractional flux basis, multiplying all terms by c_{EX}/c_{EX} to assist in algebraic simplification, and condensing components in each term around the definition of the enzyme flux control coefficient [i.e., $C_{Ex} = (\partial F/F)/(\partial c_{EX}/c_{EX})$], we can write:

$$\frac{dF}{F} = C_{E1} \frac{dc_{E1}}{c_{E1}} + C_{E2} \frac{dc_{E2}}{c_{E2}} + C_{E3} \frac{dc_{E3}}{c_{E3}} + \dots \quad (4.36)$$

Assuming first-order reaction kinetics, and recalling the connectivity of steps in a metabolic pathway, we can write:

$$\frac{dc_{E1}}{c_{E1}} = \frac{dv_1}{v_1} = \frac{dv_x}{v_x} = \frac{dF}{F} \quad (4.37)$$

The key to appreciating the relations of Equation 4.37 is to recognize linear proportionality between the change in control coefficient of a single step and its effect on the rate of reaction (v) for that step, and all other steps in the pathway that must conform to the new v . (Recall that at steady state all steps in the pathway will be operating at the same v .) This same logic of proportionality can be carried through the entire pathway with the conclusion that the overall change in pathway reaction rate (dF) scales linearly with the overall fractional change in control

coefficient C_{E_x} and is equal to the change in v for all component reactions. Denoting dc_{E_x}/c_{E_x} as δ :

$$\delta = C_{E1} \delta + C_{E2} \delta + C_{E3} \delta + \dots \quad (4.38)$$

Dividing through by δ leaves us with the final form of the summation theorem – i.e., all control coefficients for a metabolic pathway sum to 1:

$$1 = C_{E1} + C_{E2} + C_{E3} + \dots \quad (4.39)$$

The connectivity theorem recognizes that sequential enzymes in a pathway are functionally connected, and that the interactions between connected enzymes occur through common metabolites that exert their control through enzyme-specific elasticity coefficients. To examine these relationships, we begin with the recognition that it is feasible to compensate for any perturbation in enzyme concentration by changing the concentration of substrate for that enzyme. Consider the case in which a fractional change in enzyme concentration (dc_{E_x}/c_{E_x}) is balanced by a fractional change in substrate concentration (dc_j/c_j) such that there is no net change in reaction velocity. Thus:

$$\frac{dc_{E_x}}{c_{E_x}} + \varepsilon_j^x \frac{dc_j}{c_j} = \frac{dv_x}{v_x} = 0 \quad (4.40)$$

where ε_j^x is the elasticity coefficient for reaction x which utilizes substrate j . Equation 4.40 can be rearranged to provide:

$$\frac{dc_{E_x}}{c_{E_x}} = -\varepsilon_j^x \frac{dc_j}{c_j} \quad (4.41)$$

The change in c_j will affect not only the enzyme in question, but also all other enzymes connected to it through common metabolites. Consider the pathway illustrated in Figure 4.1,

whereby E_1 and E_2 are connected by the common metabolite S_2 . A change in c_2 will cause changes in the reverse reaction of E_1 (denoted by velocity v_1') and the forward reaction of E_2 (denoted by velocity v_2). The degree to which the velocities of each reaction are affected will depend on the flux control coefficient and elasticity coefficient for each enzyme. This interdependence can be best illustrated by returning to the case where a change in c_2 results in no change in flux through the pathway (i.e., $\partial F/F = 0$). In that case, Equation 4.40 can be rewritten with respect to E_1 and E_2 as:

$$0 = C_{E1} \frac{dc_{E1}}{c_{E1}} + C_{E2} \frac{dc_{E2}}{c_{E2}} \quad (4.42)$$

Using Equation 4.41 for substitution, we can write:

$$0 = -C_{E1} \varepsilon_2^{1'} \frac{dc_2}{c_2} - C_{E2} \varepsilon_2^2 \frac{dc_2}{c_2} \quad (4.43)$$

where $\varepsilon_2^{1'}$ refers to the elasticity coefficient for the reverse reaction of E_1 and ε_2^2 refers to the forward reaction of E_2 . When common variables are canceled and Equation 4.43 is rearranged, we obtain the connectivity theorem as:

$$\frac{C_{E1}}{C_{E2}} = \frac{|\varepsilon_2^2|}{|\varepsilon_2^{1'}|} \quad (4.44)$$

From the relationships of Equation 4.44 it is clear there is an inverse relationship between the flux control coefficient for an enzyme and its sensitivity to a change in substrate concentration (as transduced through the elasticity coefficient). The absolute value denotation in Equation 4.44 is required because elasticity coefficients can be positive or negative, depending on whether a change in metabolite concentration causes a fractional increase or decrease in reaction velocity.

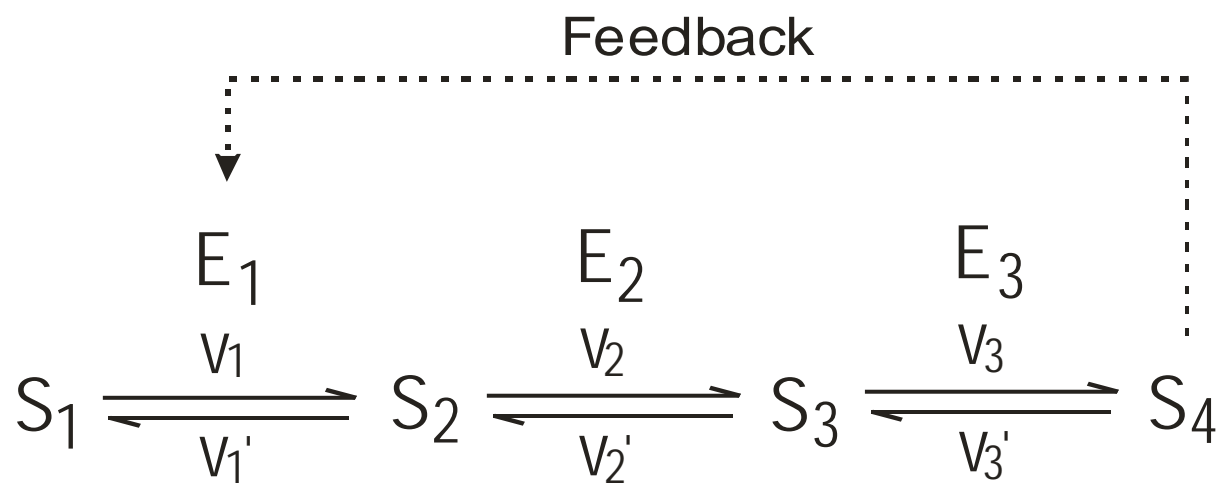


Figure 4.1 A hypothetical pathway of sequential metabolic steps demonstrating the connected relationship between successive reactions.

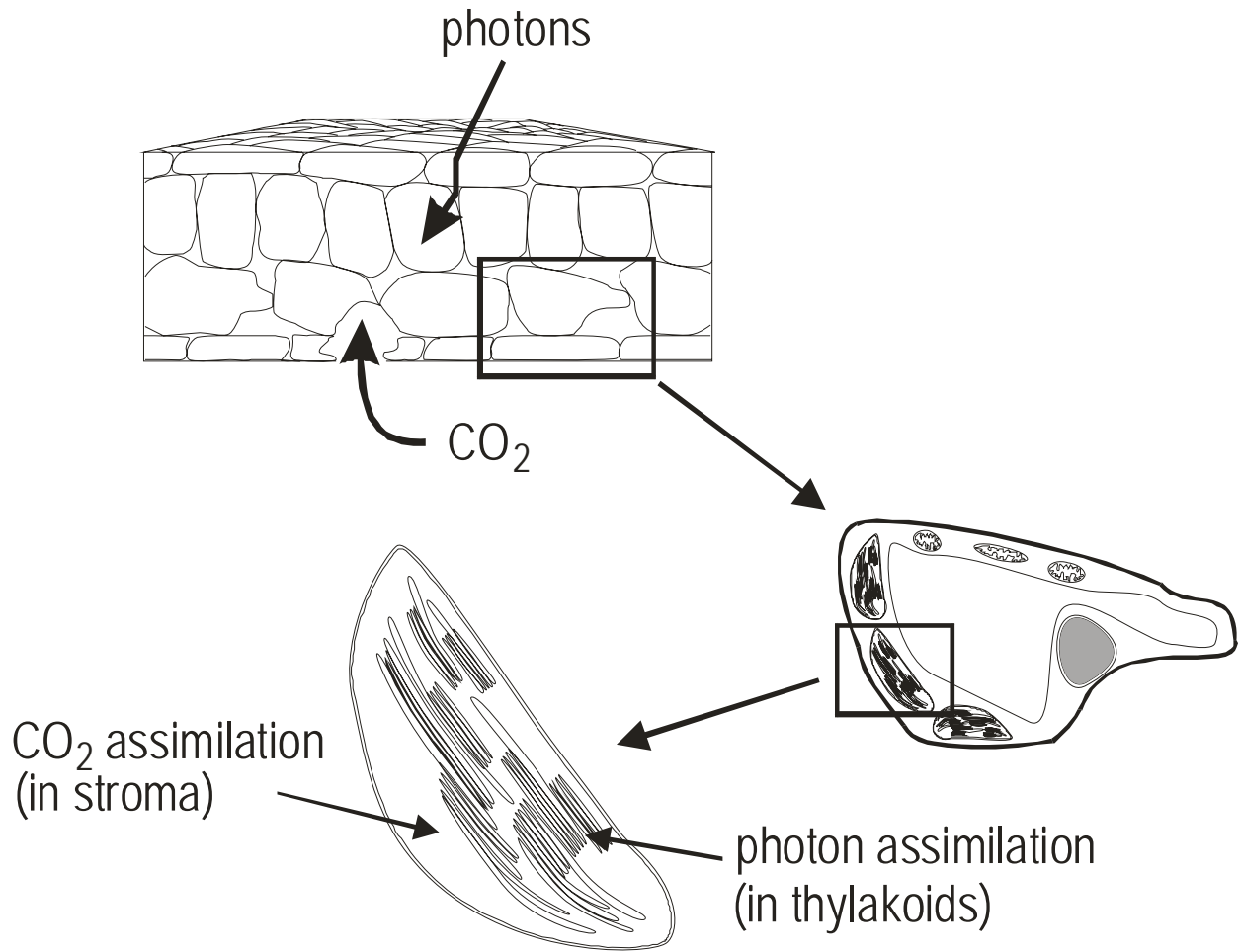


Figure 4.2 The chloroplast of terrestrial plants shown within the context of a C₃ leaf mesophyll cell.

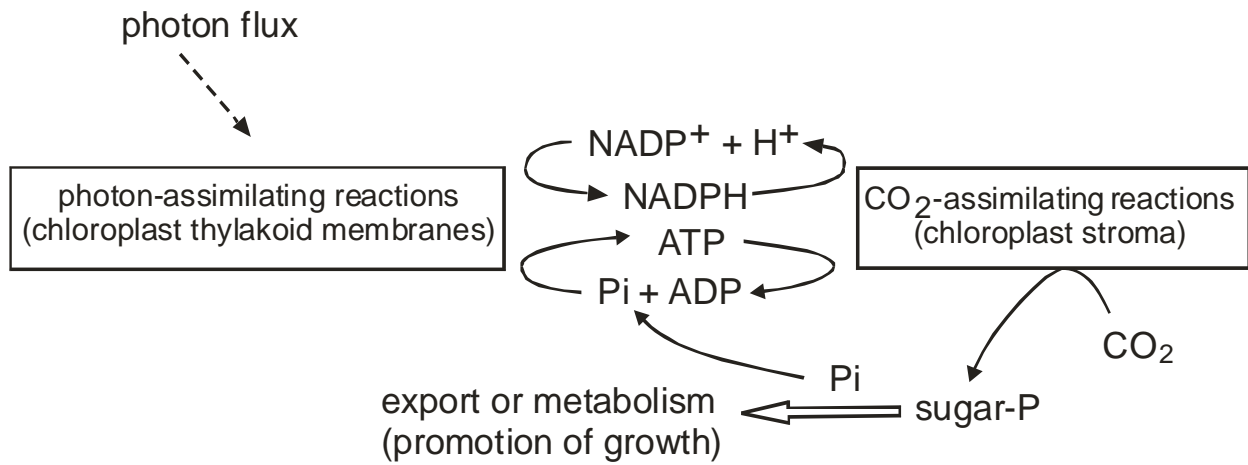


Figure 4.3 A general scheme showing interactions between the photon-assimilating reactions and CO₂ assimilating reactions in photosynthetic CO₂ assimilation.

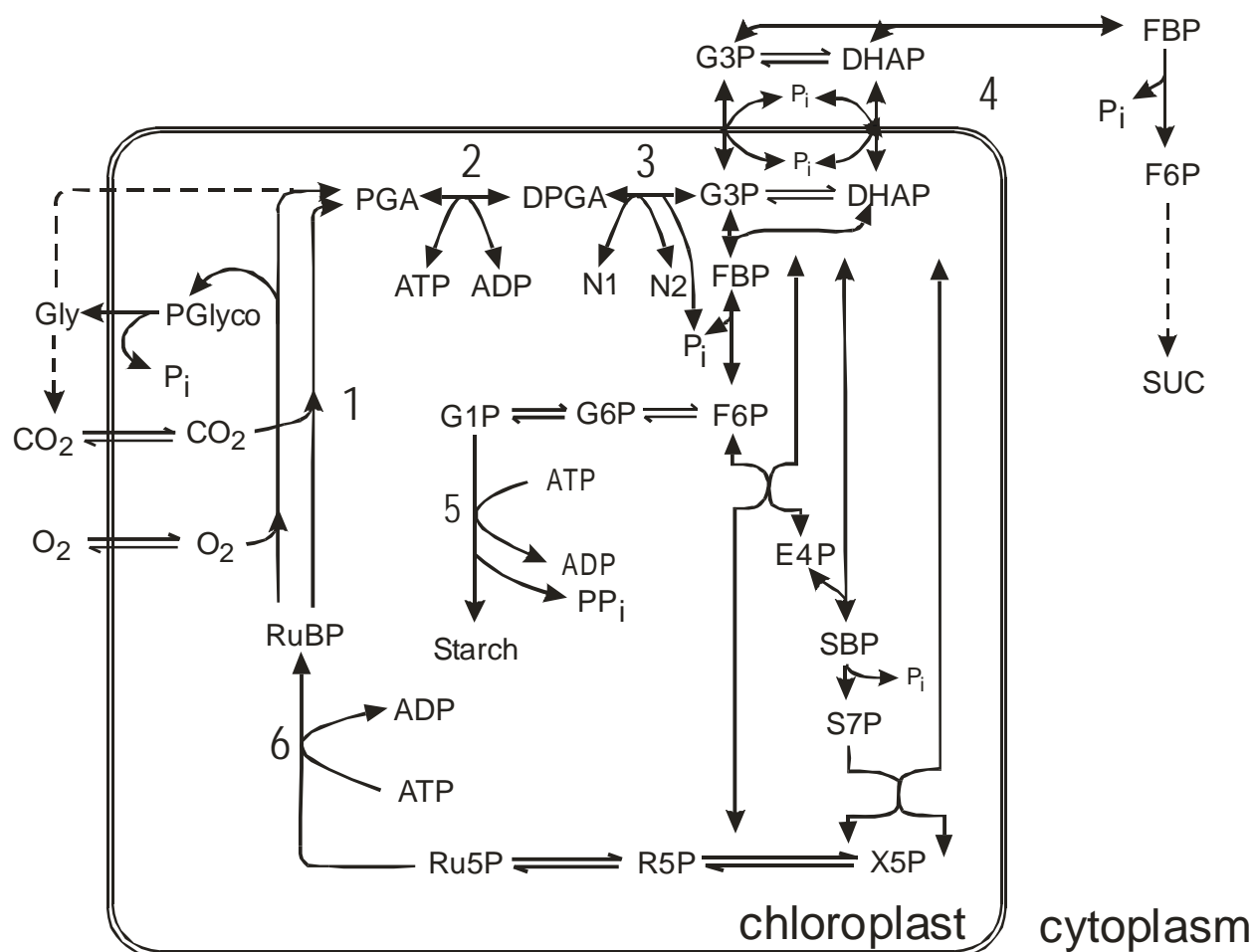


Figure 4.4 The reductive pentose phosphate pathway. The numbered steps (1 through 6) coincide with the descriptive sequence provided in the text. Abbreviations for intermediate metabolites are as follows: Gly = glycine, PGlyco = phosphoglycolate, PGA = 3-phosphoglyceric acid, DPGA = 1,3-diphosphoglyceric acid, G3P = glyceraldehyde 3-phosphate, DHAP = dihydroxyacetone phosphate, FBP = fructose 1,6-bisphosphate, F6P = fructose 6-phosphate, E4P = erythrose 4-phosphate, SBP = sedoheptulose 1,7-bisphosphate, S7P = sedoheptulose 7-phosphate, X5P = xyulose 5-phosphate, R5P = ribose 5-phosphate, Ru5P = ribulose 5-phosphate, RuBP = ribulose 1,5-bisphosphate, G1P = glucose 1-phosphate, G6P = glucose 6-phosphate, SUC = sucrose, N1 = NADP^+ , N2 = NADPH , P_i = inorganic phosphate, PP_i = inorganic pyrophosphate. (Redrawn from Woodrow and Mott, 1993).

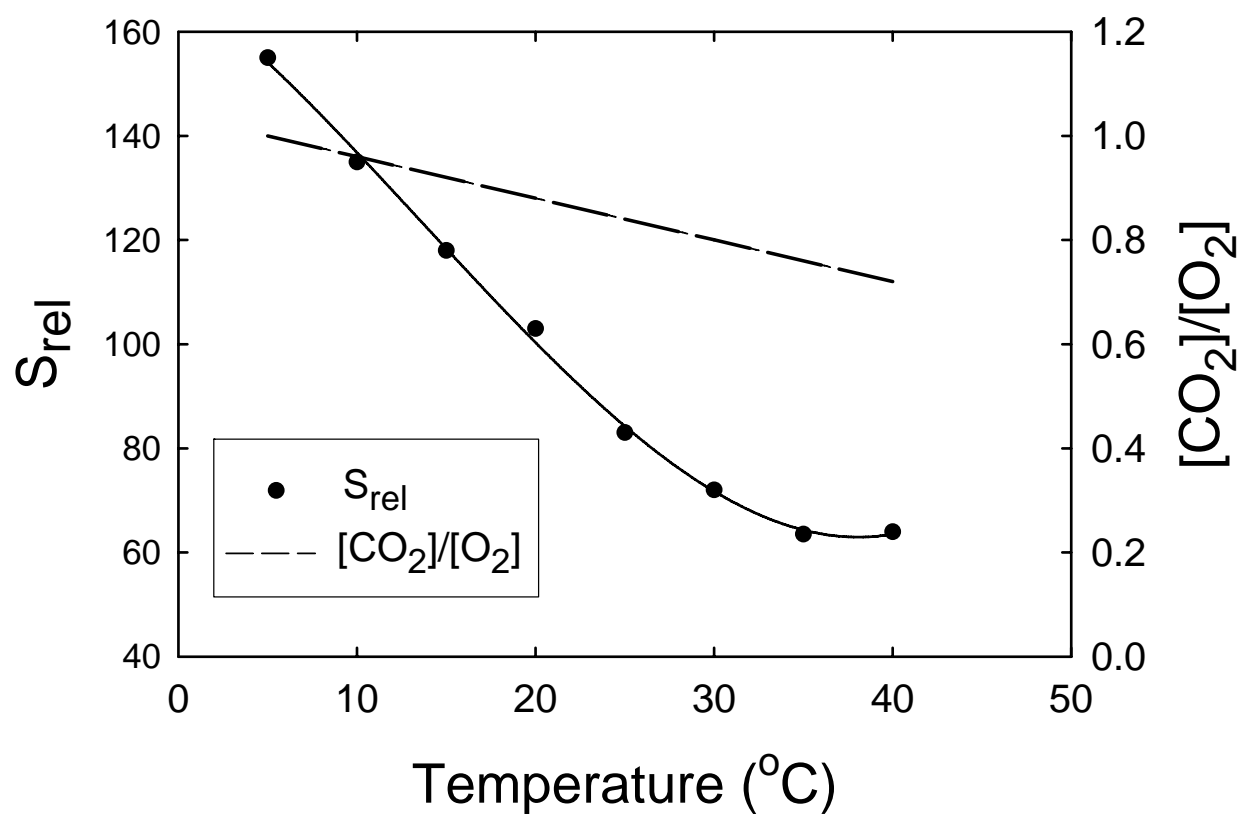


Figure 4.5 Relationships among temperature, the Rubisco specificity factor (S_{rel}) and the relative concentrations of CO_2 and O_2 in solution. (Redrawn from Jordan and Ogren, 1984; and Sage and Reid, 1998).

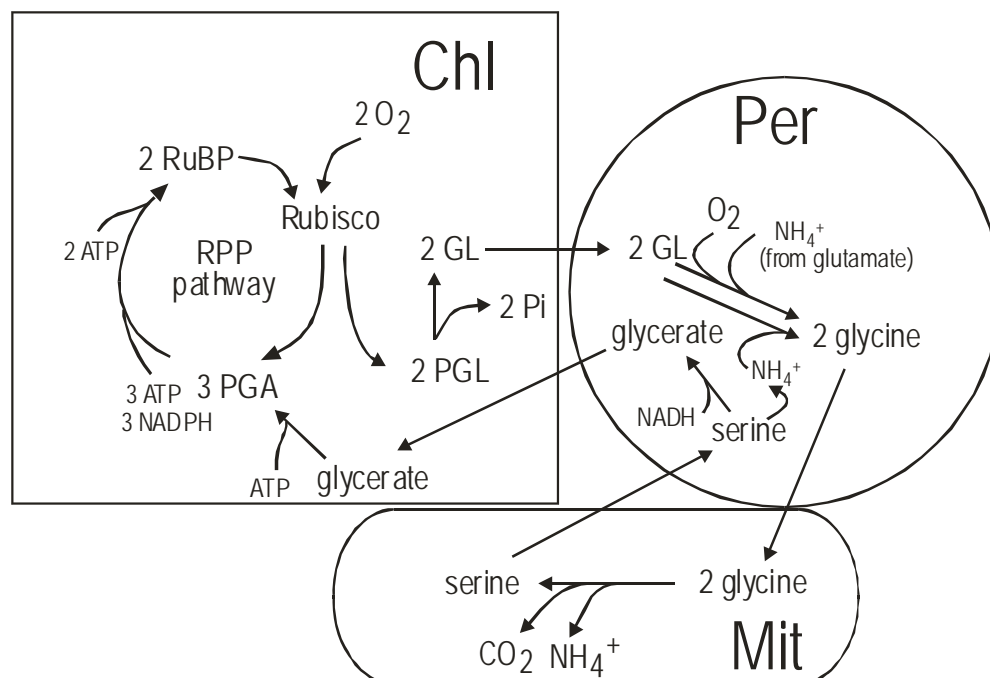
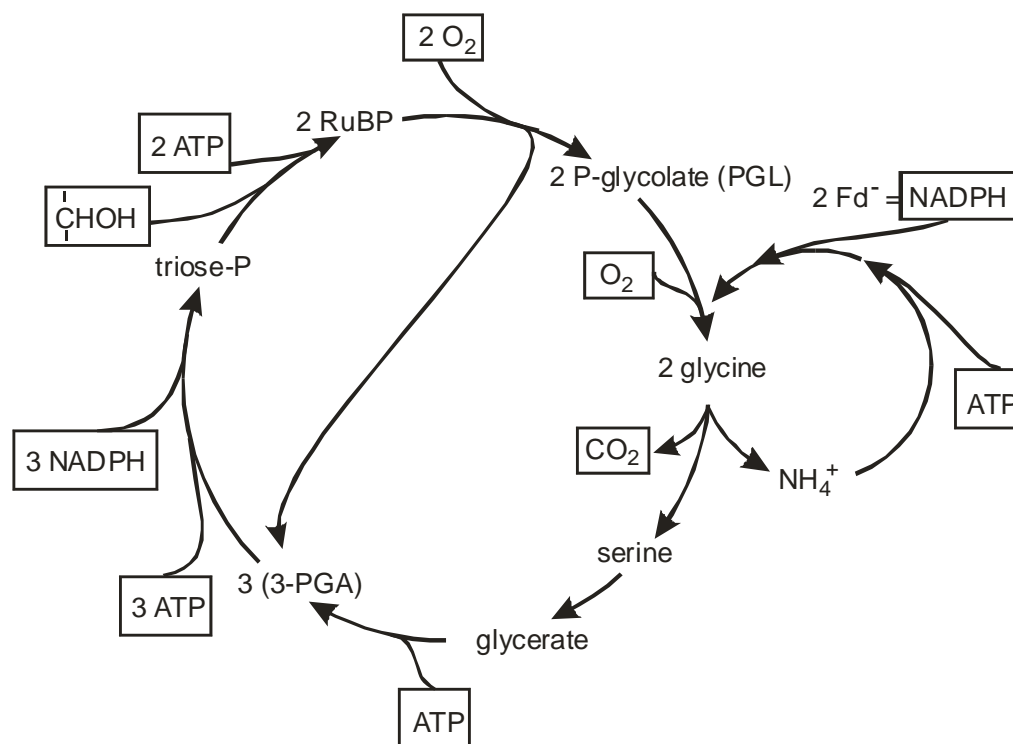


Figure 4.6 The photorespiratory pathway involving three cellular organelles – chloroplasts (Chl), peroxisomes (Per), and mitochondria (Mit). Photorespiration is initiated when the oxygenation of RuBP, which is catalyzed by Rubisco, produces phosphoglycolate (PGL) in the chloroplast. The phosphoglycolate is converted to glycolate and transported to the peroxisome where it is converted to the amino acid, glycine. Glycine is transported to the mitochondrion where two glycines (each with 2 carbons) are combined to form one serine (with 3 carbon atoms) and one CO₂ molecule. The serine is then transported back through the peroxisome where it is converted to glycerate, and then back into the chloroplast, where it is converted to phosphoglycerate (PGA), which then enters the RPP pathway. Thus, photorespiration provides an effective metabolic means of recycling some of the carbon atoms in PGL, which is produced through oxygenation of RuBP, to form a compound, PGA, capable of re-entering the RPP pathway.



Summary: -3.5 ATP, -2 NADPH, -1.5 O₂, + 0.5 CO₂ per oxygenation

Figure 4.7 Stoichiometric relationships of the photorespiratory carbon oxidation (PCO) cycle. For summation purposes, the stoichiometry is determined on the basis of two oxygenations. Important stoichiometric steps are: (1) the consumption of 1 ATP and 1 NADPH to re-assimilate NH₄⁺; (2) the production of 1 CO₂ in the conversion of two glycines to one serine; (3) the consumption of 1 ATP to convert glycerate to P-glycerate (PGA); (4) the consumption of 3 ATP and 3 NADPH to reduce the 3 PGA molecules (two produced during the oxygenation and one produced from the oxidation of two PGL molecules to form one PGA molecule); (5) the consumption of 2 ATP in the final regeneration of RuBP; and (6) the required consumption of one unit of reduced carbon to maintain carbon balance in the cycle. This latter step reflects the fact that 25% of the carbon that enters the photorespiratory pathway is lost as CO₂; only 75% is recycled back to the RPP pathway. Thus, the stoichiometry must reflect the continual input of 1 unit of reduced carbon per two oxygenations to maintain steady-state balance. (Redrawn from Berry and Farquhar, 1978).

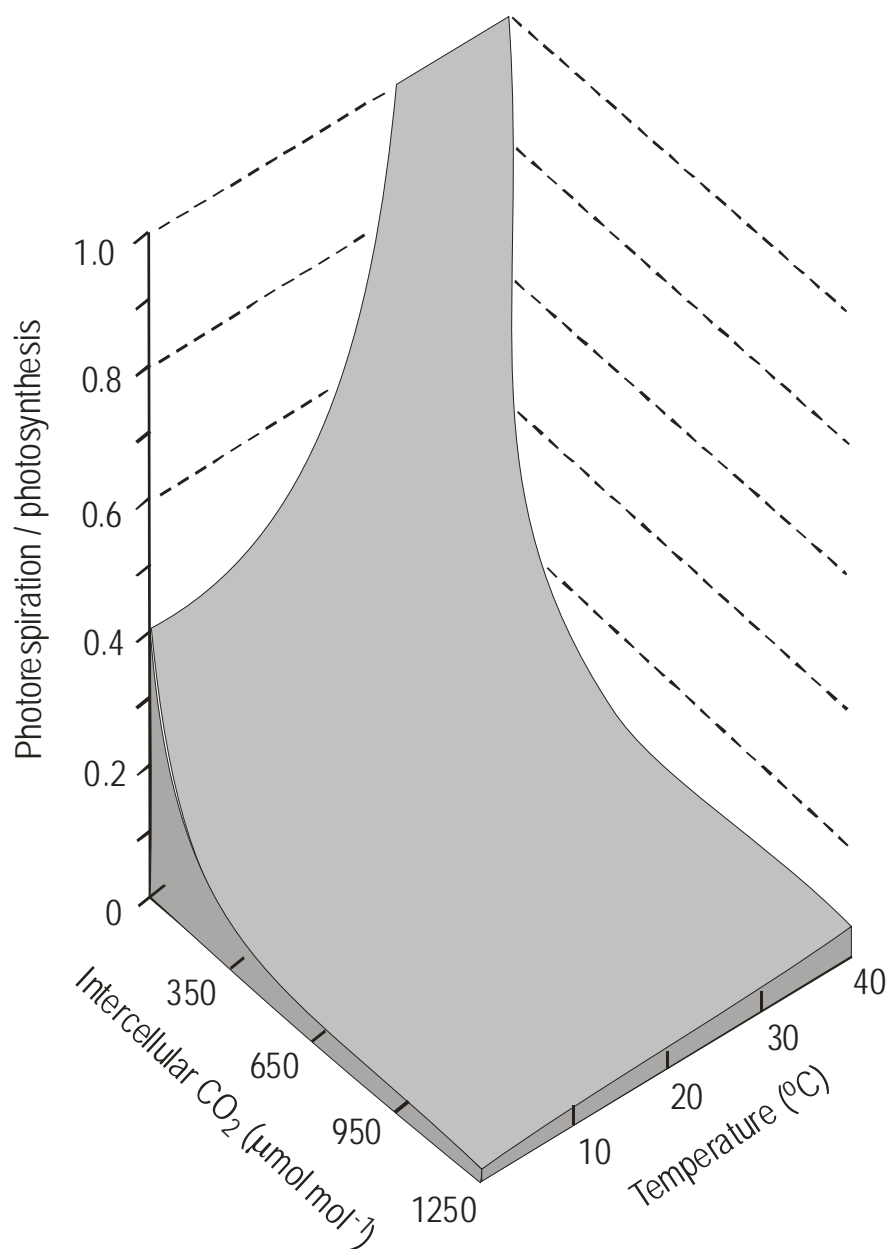


Figure 4.8 The relationships among the ratio of photorespiration to photosynthesis, leaf temperature, and leaf intercellular CO₂ mole fraction. The photorespiration to photosynthesis ratio reaches a limit of 1.0 because it is assumed that photorespiration rates cannot be sustained over time if the rate of CO₂ loss is greater than the rate of CO₂ uptake. (Redrawn from Sage and Reid, 1998).

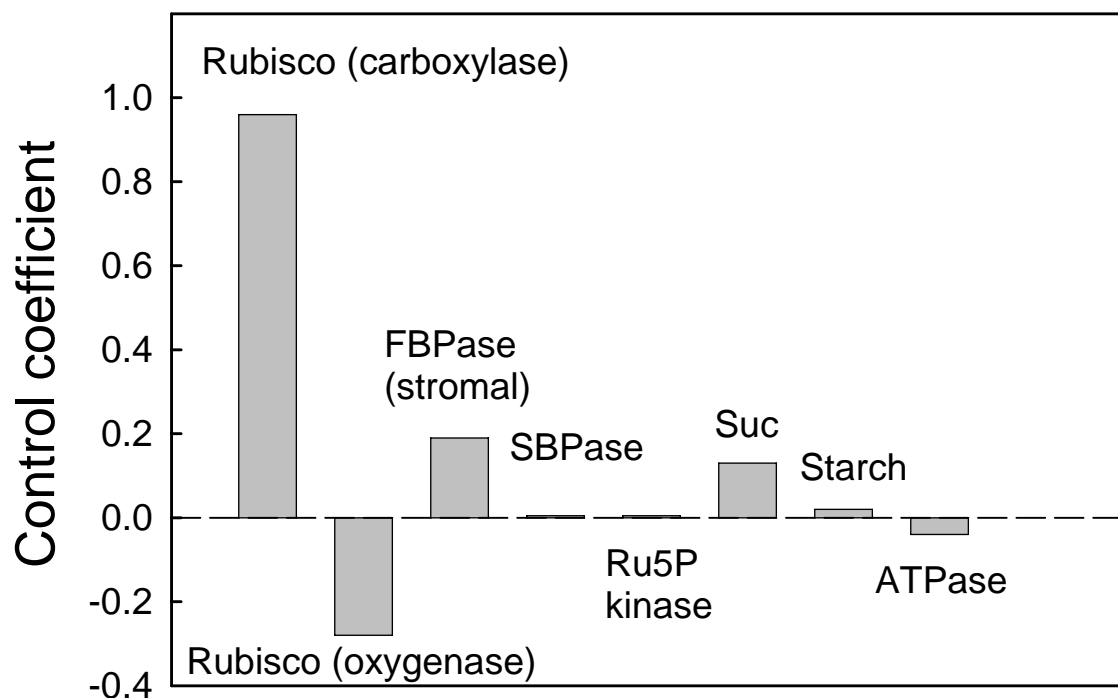


Figure 4.9 Calculated steady-state, flux control coefficients for several steps of the RPP pathway in the presence of normal atmospheric CO₂ concentration (approx. 345 μmol mol⁻¹). Suc and Starch refer to the composite processes of sucrose synthesis and starch synthesis, respectively, rather than to single enzyme steps. (Redrawn from Woodrow and Mott, 1993).

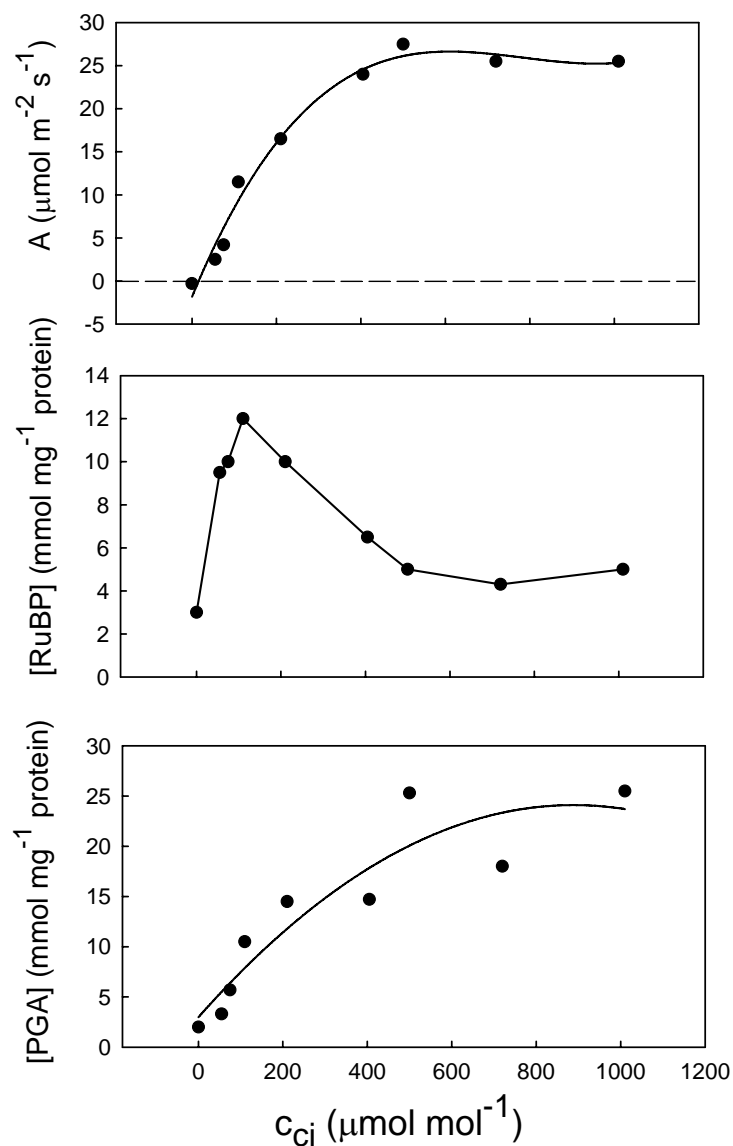


Figure 4.10 The relationship of leaf net CO_2 assimilation rate (A), extracted RuBP concentration, and extracted PGA concentration to the intercellular CO_2 concentration (c_{ci}) for leaves of *Phaseolus vulgaris* (common pole bean). As CO_2 concentration increases, the velocity of RuBP carboxylation increases (as reflected in higher values for A), the concentration of RuBP, the CO_2 acceptor molecule, decreases, and the concentration of PGA, the first stable product of RuBP carboxylation, increases. (Redrawn from Badger et al., 1984).

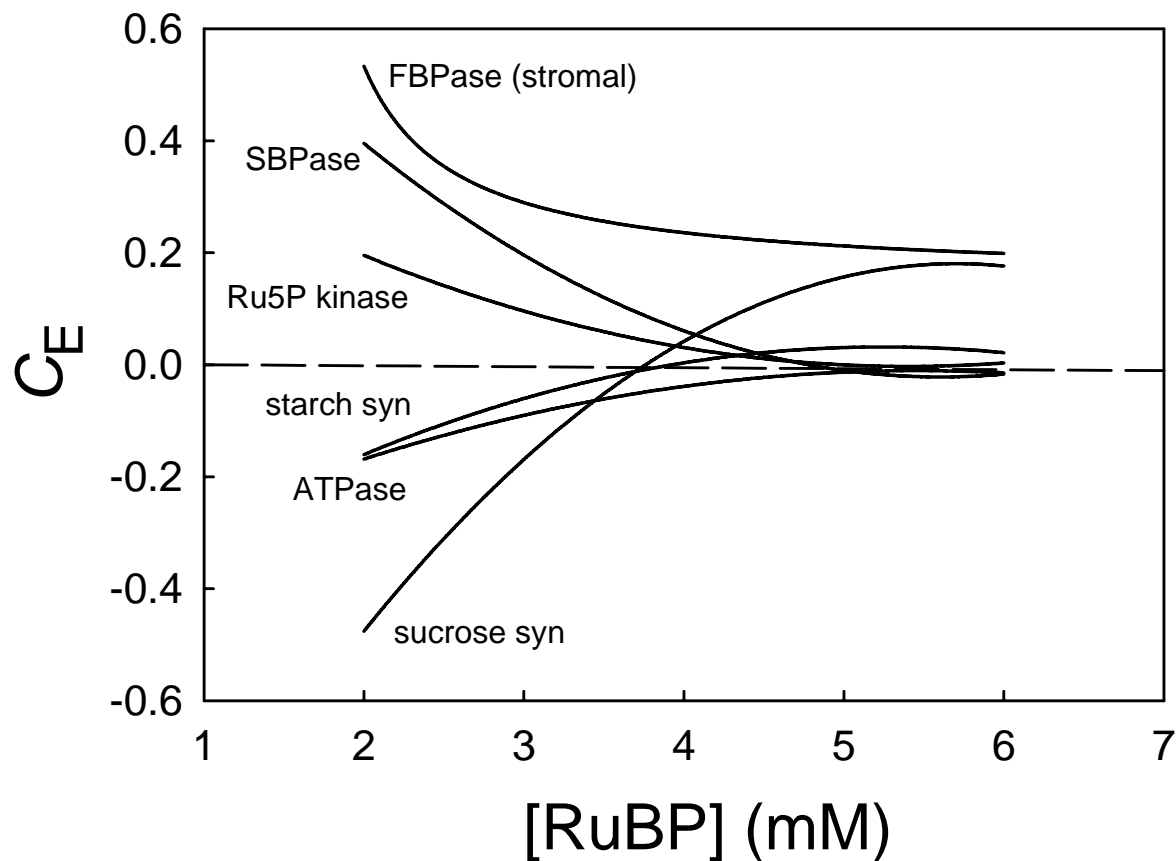


Figure 4.11 Changes in the control coefficients (C_E) of enzymes in the RPP pathway associated with processes other than Rubisco carboxylation and oxygenation as a function of stromal RuBP concentration. Note that the control coefficients of those enzymes that are involved in the regeneration of RuBP (FBPase, SBPase, and Ru5P kinase) exhibit high control over flux at low RuBP concentrations. (Redrawn from Woodrow and Mott 1993).

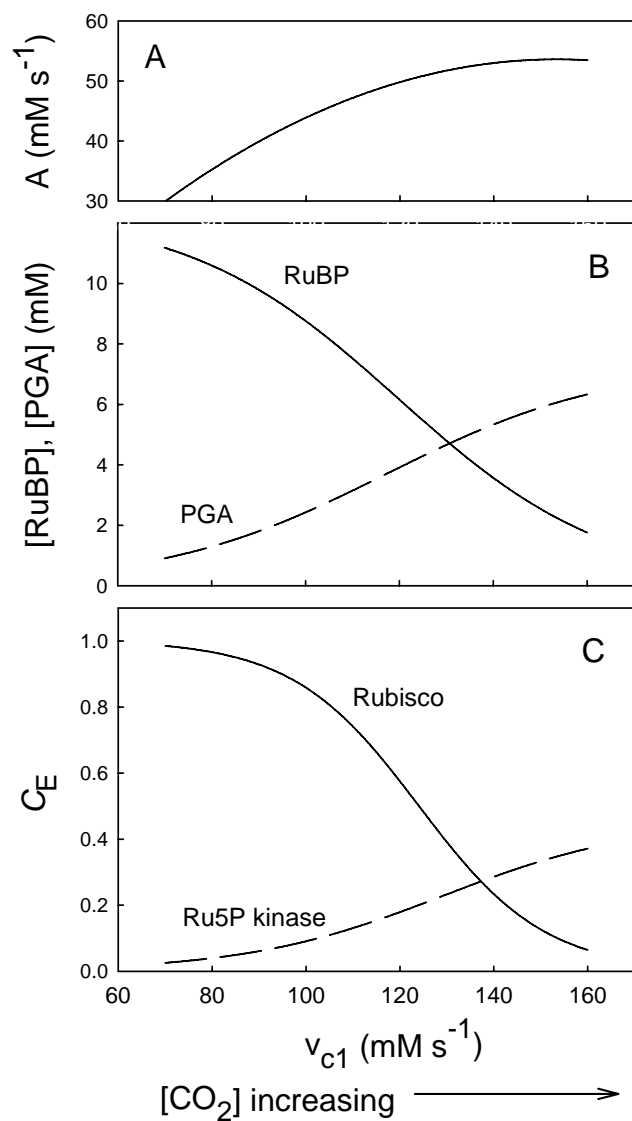


Figure 4.12 Modeled changes in the net CO_2 assimilation rate (A) by the RPP pathway (panel A), the stromal concentrations of RuBP and PGA (panel B), and control coefficient (C_E) for Rubisco and Ru5P kinase (panel C) as a function of the Rubisco carboxylation rate (v_{c1}). The model was driven by increasing CO_2 concentration, which forced the increase in v_{c1} . Redrawn from Woodrow (1986).

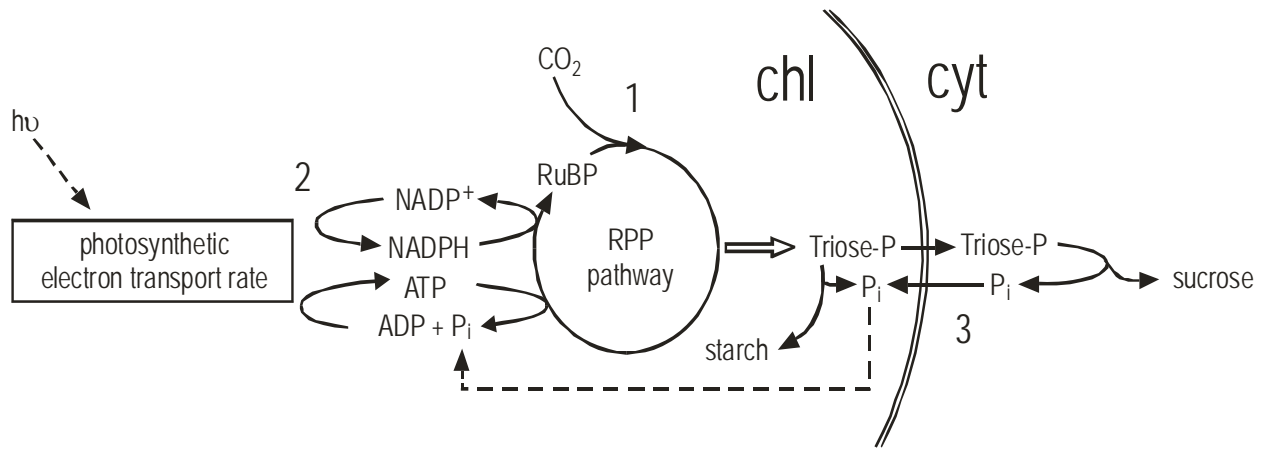


Figure 4.13 Schematic relationships within the RPP pathway demonstrating the three primary constraints to RuBP carboxylation rate upon which the most commonly-used biochemical models of CO₂ assimilation rate are based. 1, the constraint reflected in CO₂ availability and the kinetic capacity of RuBP carboxylase to assimilate CO₂ (i.e., Rubisco-limited state); 2, the constraint reflected in the photosynthetic electron transport rate and its capacity to provide ATP and NADPH in order to regenerate RuBP (i.e., the RuBP-limited state); 3, the constraint reflected in the capacity for the assimilation of triose phosphate sugars and the freeing of inorganic phosphate (P_i) (i.e., the triose-phosphate utilization (TPU)-limited state).

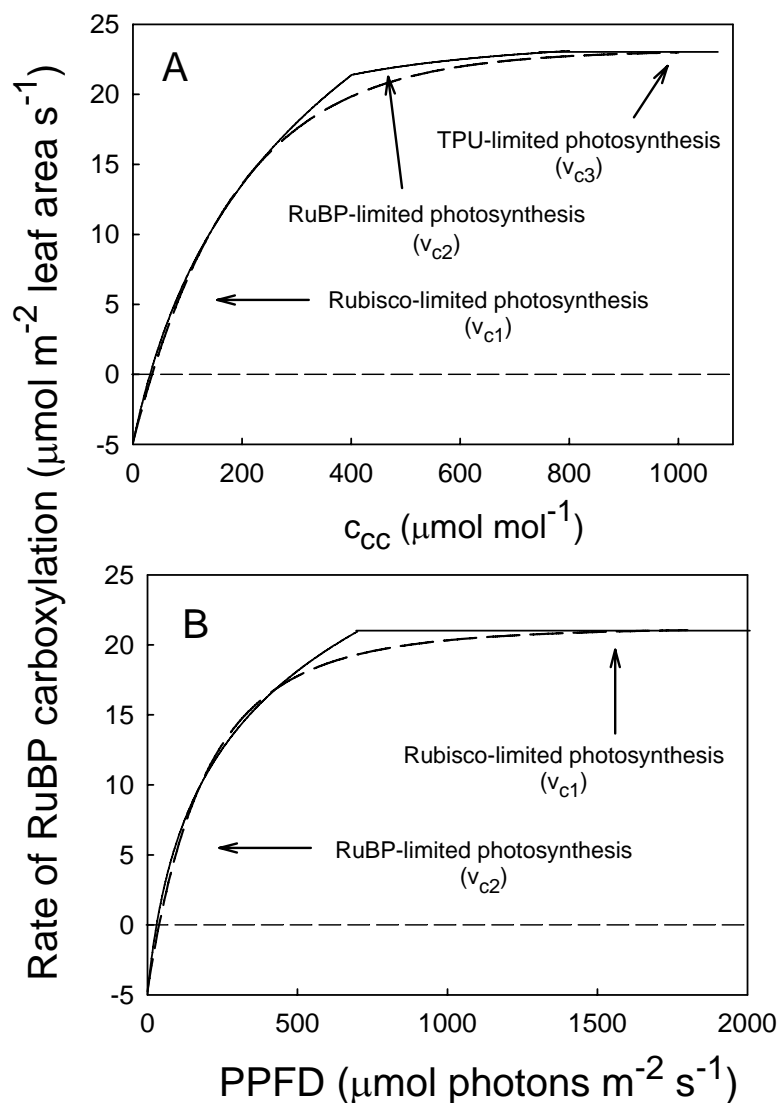


Figure 4.14 Diagrammatic representations of the RuBP carboxylation rate as it responds to CO_2 concentration in the chloroplast (c_{cc}) or photosynthetic photon flux density (PPFD). The terms v_{c1} , v_{c2} , and v_{c3} refer to the rate of RuBP carboxylation under conditions of Rubisco limitation, RuBP-regeneration limitation, or triose-phosphate utilization limitation, respectively (see text for details). The broken lines represent the type of response typically observed when observations are made with C_3 leaves. The solid lines represent the minimum of three possible limitations, which reflects the modeling approach of Farquhar et al. (1980b) in its simplest form.

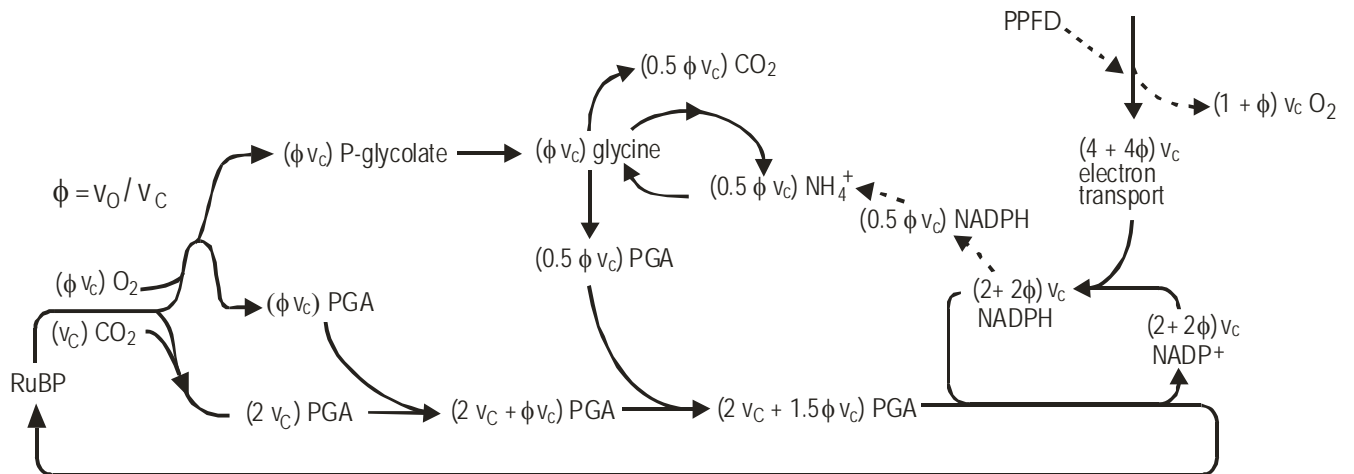


Figure 4.15 Stoichiometric relations in the RPP pathway expressed as functions of the rate of carboxylation (v_c) and the ratio (ϕ) of oxygenation to carboxylation rates. The stoichiometry is used to relate the rate of production of major products in the RPP and PCO pathways to v_c . As an example, the rate of PGA production directly from carboxylation by Rubisco, early in the pathway, is $(2 v_c)$. The rate of total PGA production, from both carboxylation and oxygenation is $(2 v_c + 1.5\phi v_c)$. (Redrawn from Farquhar and von Caemmerer, 1982).

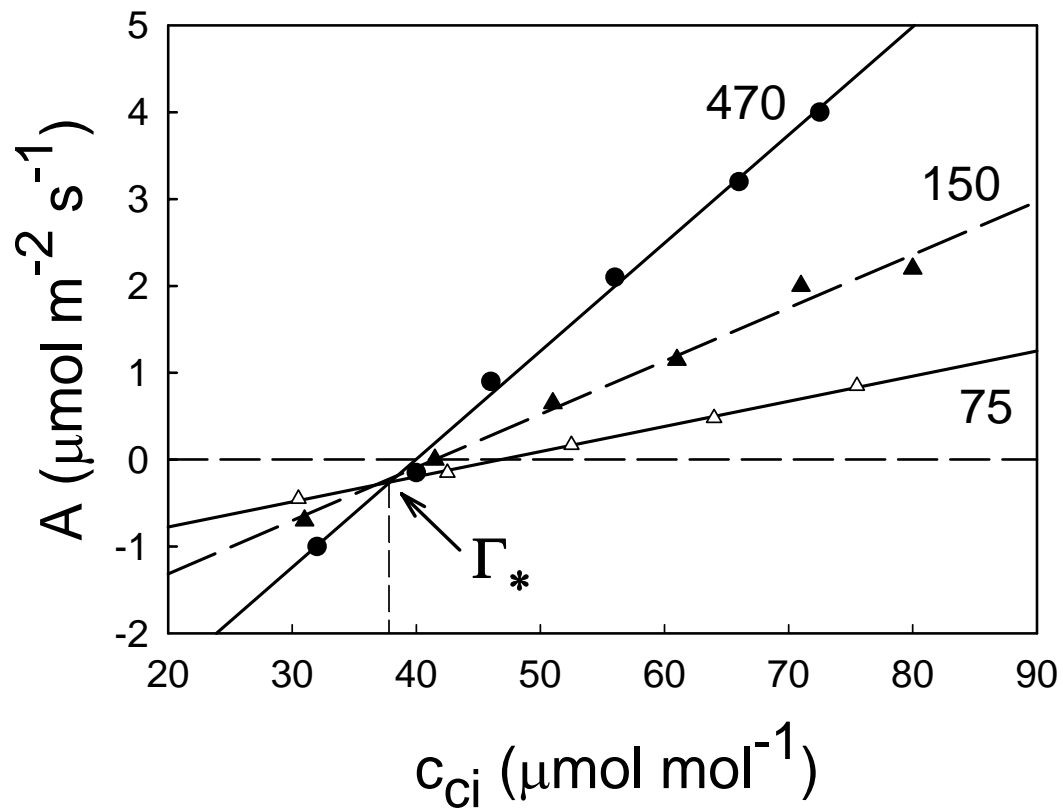


Figure 4.16 Rate of net CO_2 assimilation (A) in spinach leaves as a function of intercellular CO_2 concentration (c_{ci}) at three different PPFD values. The light-independent intersection of the three lines is taken as the CO_2 compensation point in the absence of TCA-cycle respiration (Γ^*). (Redrawn from Brooks and Farquhar 1985).

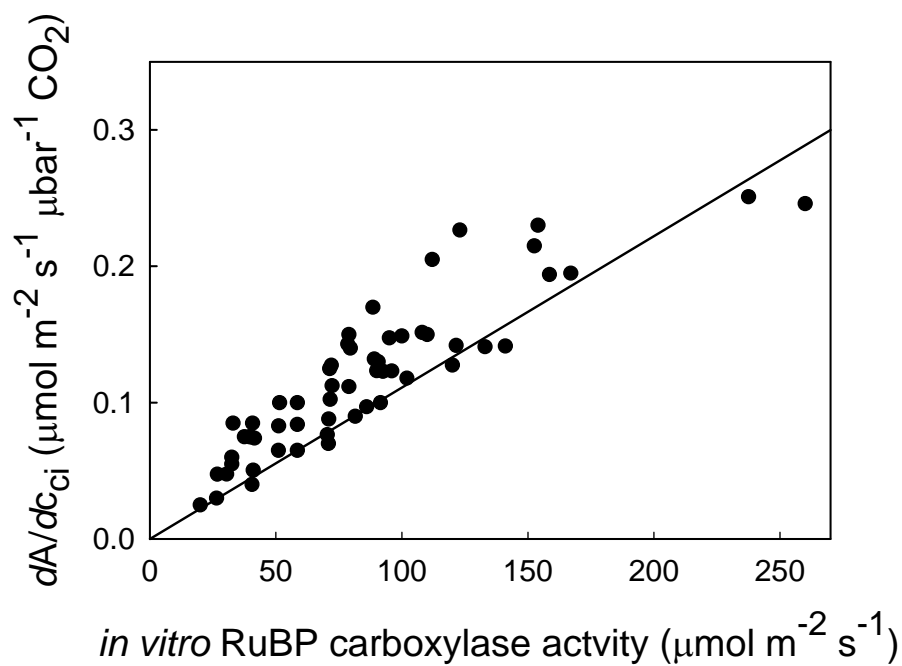


Figure 4.17 The relation between the initial slope of the $A:c_{ci}$ response measured on intact leaves of *Phaseolus vulgaris* and the maximum RuBP carboxylase activity extracted from the same leaves. The line represents the relation modeled from Equation 4.17 assuming that the extracted activity measured *in vitro* equals V_{cmax} . The difference between the modeled and measured values for dA/dc_{ci} is probably due to incomplete extraction of the enzyme activity from the leaves. (Redrawn from von Caemmerer and Farquhar 1981).

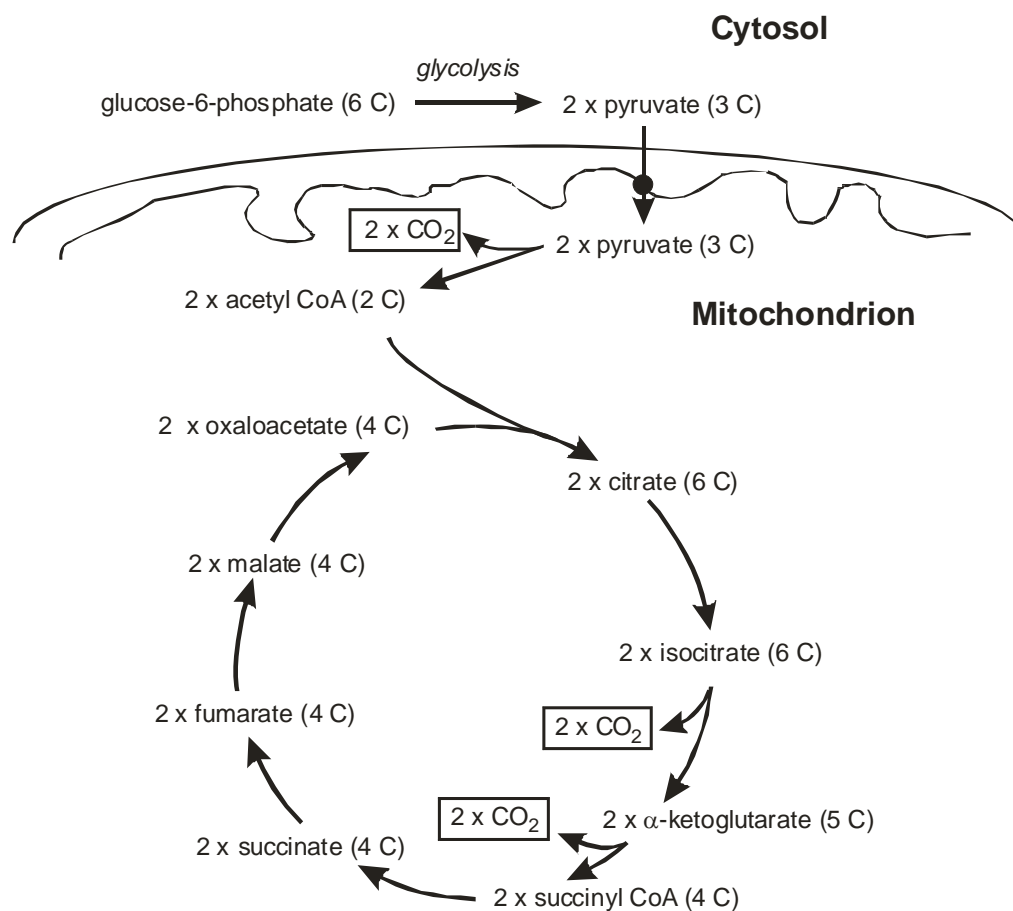


Figure 4.18 Carbon fluxes in the mitochondrial TCA pathway (Krebs cycle) of plant cells. Beginning with glucose 6-phosphate, the catalyzed reactions of glycolysis in the cytosol, and pyruvate dehydrogenase and the TCA cycle in the mitochondrion result in the oxidation of six carbon atoms to form CO₂. Energetic fluxes in the pathway are not explicitly considered, although it should be recognized that primary energetic products of the pathway include high-energy electron carriers (NADH and FADH₂) and ATP, both of which reflect oxidative free energy extraction from pyruvate.

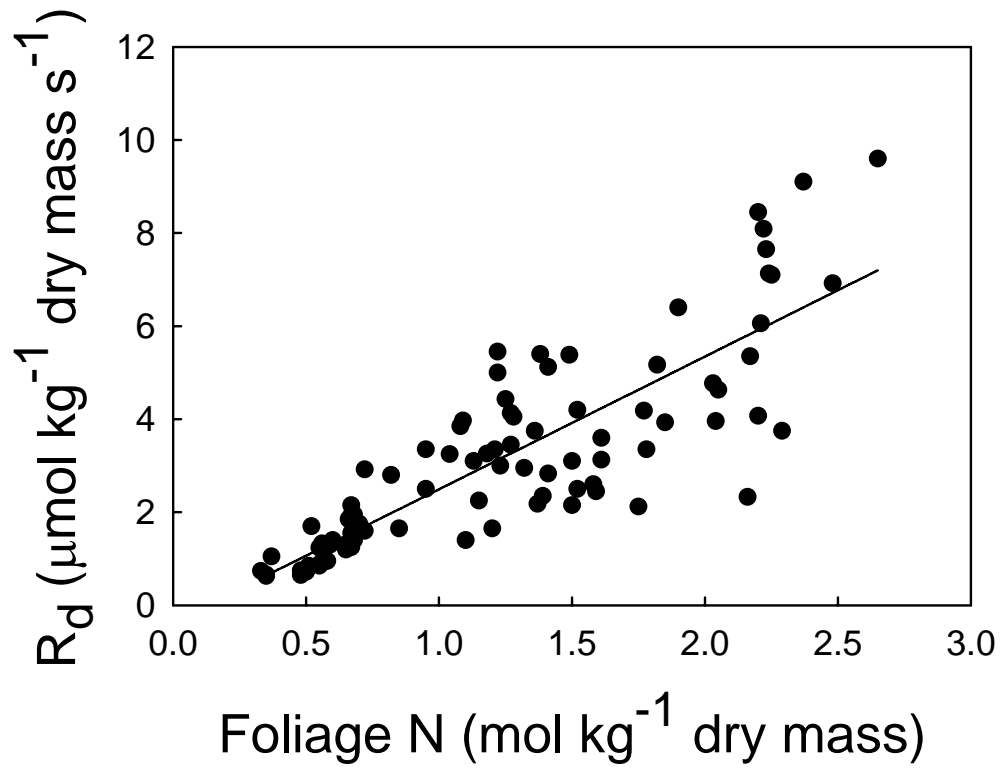


Figure 4.19 Linear relationship between foliar N concentration and dark respiration rate in 14 subalpine and boreal forest trees and shrubs. (Redrawn from Ryan, 1995).

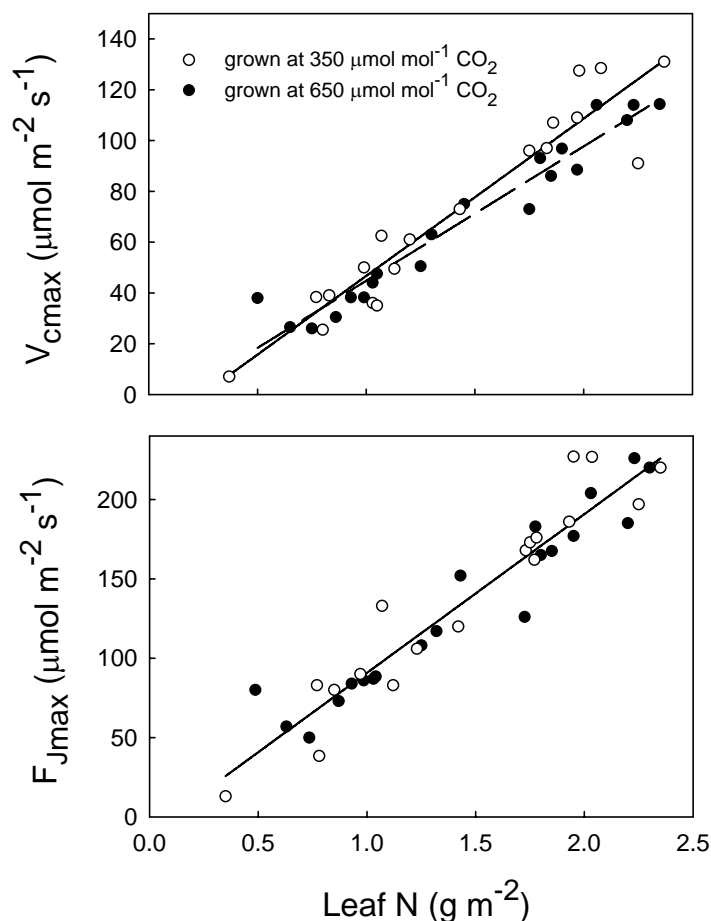


Figure 4.20 The relationship between the maximum rate of RuBP carboxylation ($V_{C_{max}}$) the maximum rate of electron transport ($F_{J_{max}}$) and leaf N concentration in leaves of *Gossypium hirsutum* (cotton). The plants used in this analysis were grown at two different atmospheric CO_2 concentrations. Separate regressions are presented for the plants from the different CO_2 treatments in the case of $V_{C_{max}}$. In the case of $F_{J_{max}}$, all values were analyzed with same regression. Regression lines were: $V_{C_{max}(350)} = 60.0 N - 9.6$ ($r^2 = 0.90$); $V_{C_{max}(650)} = 52.8 N - 6.6$ ($r^2 = 0.94$); $F_{J_{max}} = 98.1 N - 4.6$ ($r^2 = 0.91$). (Redrawn from Harley et al., 1992b).

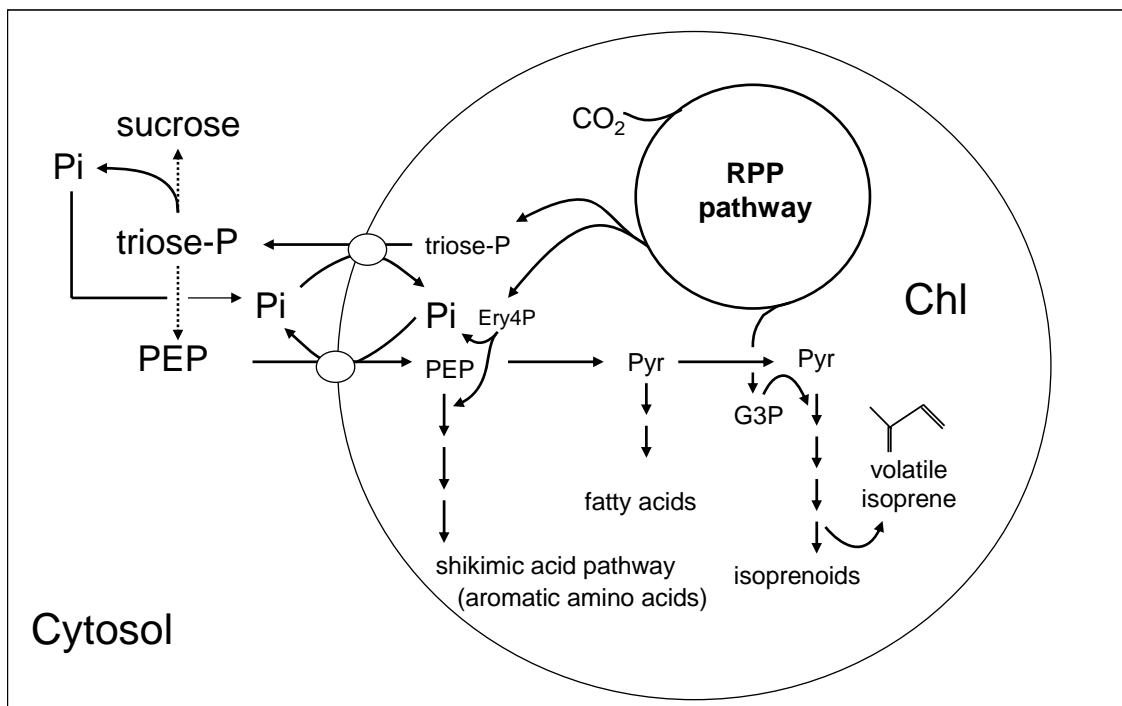


Figure 4.21. General scheme showing the flow of carbon from the photosynthetic RPP pathway in the chloroplast (Chl) to volatile isoprene that is lost to the atmosphere. Two substrates are required for the 1-deoxy-D-xyulose-5-phosphate (DOXP) pathway that is responsible for the synthesis of isoprene: pyruvate (pyr) which is derived from phosphoenolpyruvate phosphate (PEP) imported from the cytosol and glyceraldehyde 3-phosphate (G3P), which is a product of the RPP pathway. Pi = inorganic phosphate

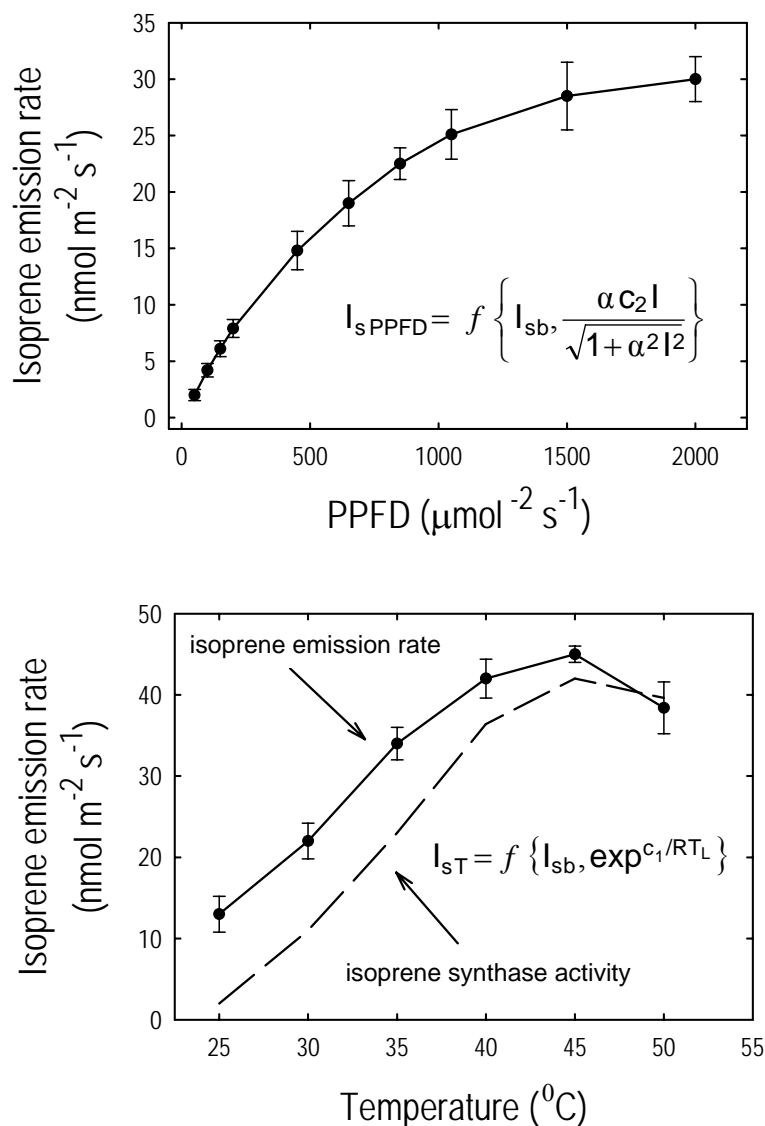


Figure 4.22. Upper. Relation between leaf isoprene emission rate and photosynthetic photon flux density (PPFD) for leaves of aspen trees. The modeled response is shown in general form as describing a rectangular hyperbola dependent on the base isoprene emission (I_{sb}), the initial slope of the light response (α) and the incident PPFD (I). **Bottom.** Relation between leaf isoprene emission rate, the activity of the enzyme isoprene synthase and temperature. The modeled response is shown in general form as describing an exponential (Arrhenius-type) relation dependent on I_{sb} and leaf temperature (T_L).

Box 4.1 Response of photosynthesis in C₃ plants to elevated atmospheric CO₂ concentration

Over the past 130 years the earth system has experienced a significant increase in the atmospheric CO₂ concentration (c_{ca}) due to human activities. Since the late 19th Century, the production of CO₂ as a pollutant from fossil fuel combustion and biomass burning has caused c_{ca} to increase by approximately 40%, and it continues to increase at the rate of 2-3 $\mu\text{mol mol}^{-1}$ per year (about 4.1 Pg of CO₂ per year) (Canadell et al. 2007). Given that the K_c of Rubisco is in the same range as c_{ca} , past increases in c_{ca} have undoubtedly stimulated C₃ plant photosynthesis. Using the biochemical model of photosynthesis described in this chapter we can estimate that in the past 130 years C₃ photosynthesis rates have increased by 30% and 9% when limited by Rubisco (v_{c1}) or RuBP regeneration (v_{c2}), respectively. Because the competition between carboxylation and oxygenation increases at higher temperatures, the photosynthetic effect of an increase in c_{ca} has been enhanced in warmer climates (Fig. B.4.1.1).

In addition to direct effects on Rubisco activity, the growth of plants at an elevated c_{ca} has longer-term influences on photosynthesis. For example, growth at a c_{ca} equal to twice the current level causes leaf carbohydrate concentrations to increase by 50% in some species (Long and Drake 1992). Growth at elevated c_{ca} also causes a reduction in the genetic transcription of genes for photosynthetic enzymes, including Rubisco activase (van Oosten et al. 1994), carbonic anhydrase (Majeau and Coleman 1996), and Rubisco (Sage et al. 1989, Moore et al. 1998). In fact, it is the enzymes that support the RPP pathway that are most reduced in activity when plants are grown under elevated c_{ca} (Nie et al. 1995a, 1995b). A model has been proposed in which an imbalance between the rate of photosynthetic CO₂ assimilation and the rate at which sugars are utilized for growth triggers a negative feedback that controls the expression of photosynthetic genes (Moore et al. 1999, Fig. B.4.1.2). Despite a downregulation in the expression of photosynthetic enzymes when plants are grown at elevated c_{ca} , the overall growth rate of the plants is increased. When plants are grown at elevated CO₂ concentrations in Free Air CO₂ Exchange (FACE) experiments, and therefore under relatively natural environmental conditions, the reduction in Rubisco protein is more than compensated by the higher CO₂ substrate concentration (Long et al. 2004, Nowak et al. 2004). Thus, on theoretical grounds, global increases in c_{ca} should cause increases in primary production. There are reasons why these theoretical predictions may not match observations in real ecosystems. For example,

nutrient and climate limitations to plant growth may accompany elevated c_{ca} causing unanticipated stress or nutrient imbalances.

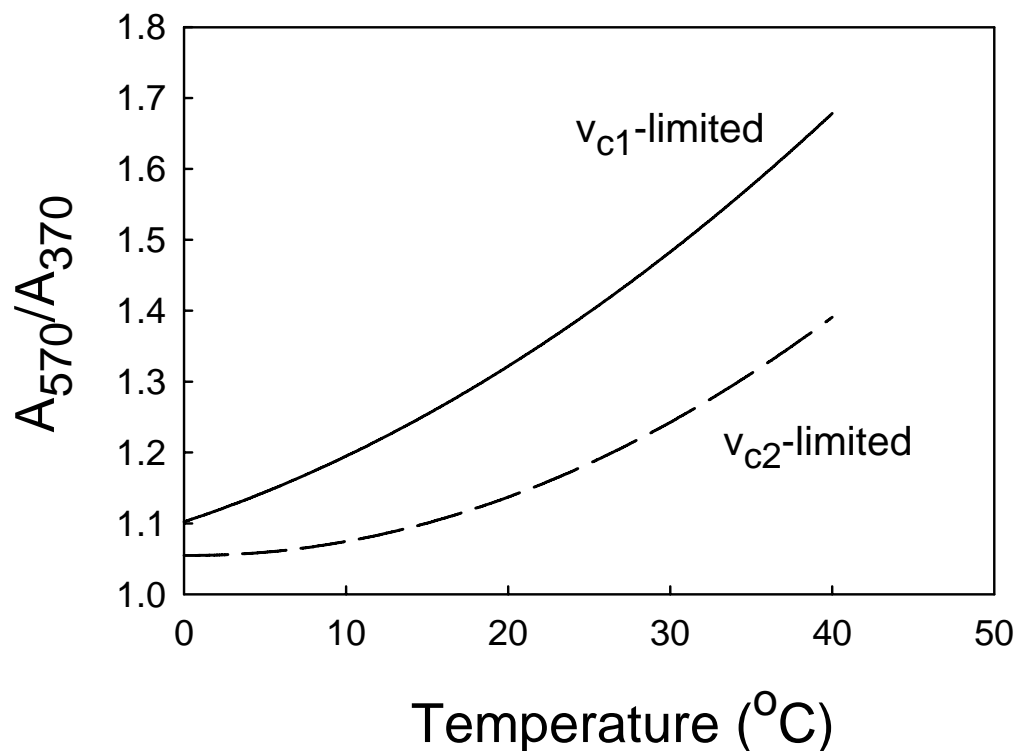


Figure B.4.1.1. The potential increase in net CO_2 assimilation rate in C_3 plants with an assumed c_{ca} of $370 \mu\text{mol mol}^{-1}$ versus $570 \mu\text{mol mol}^{-1}$ across a range of temperatures. We assumed $V_{c_{max}}$ of $120 \mu\text{mol m}^{-2} \text{s}^{-1}$ at 25°C and c_{ci}/c_{ca} of 0.6. The increase in v_{c1} at higher CO_2 concentration is due to the effect of a higher substrate concentration on the velocity of Rubisco and a decrease in the competitive interaction between CO_2 and O_2 at the active site of Rubisco. The increase in v_{c2} at higher CO_2 concentration is due to the reduction in ATP and NADPH required for photorespiration at the higher CO_2 concentration, and therefore an increase in the potential to regenerate RuBP. (Redrawn from Long et al. 2004.)

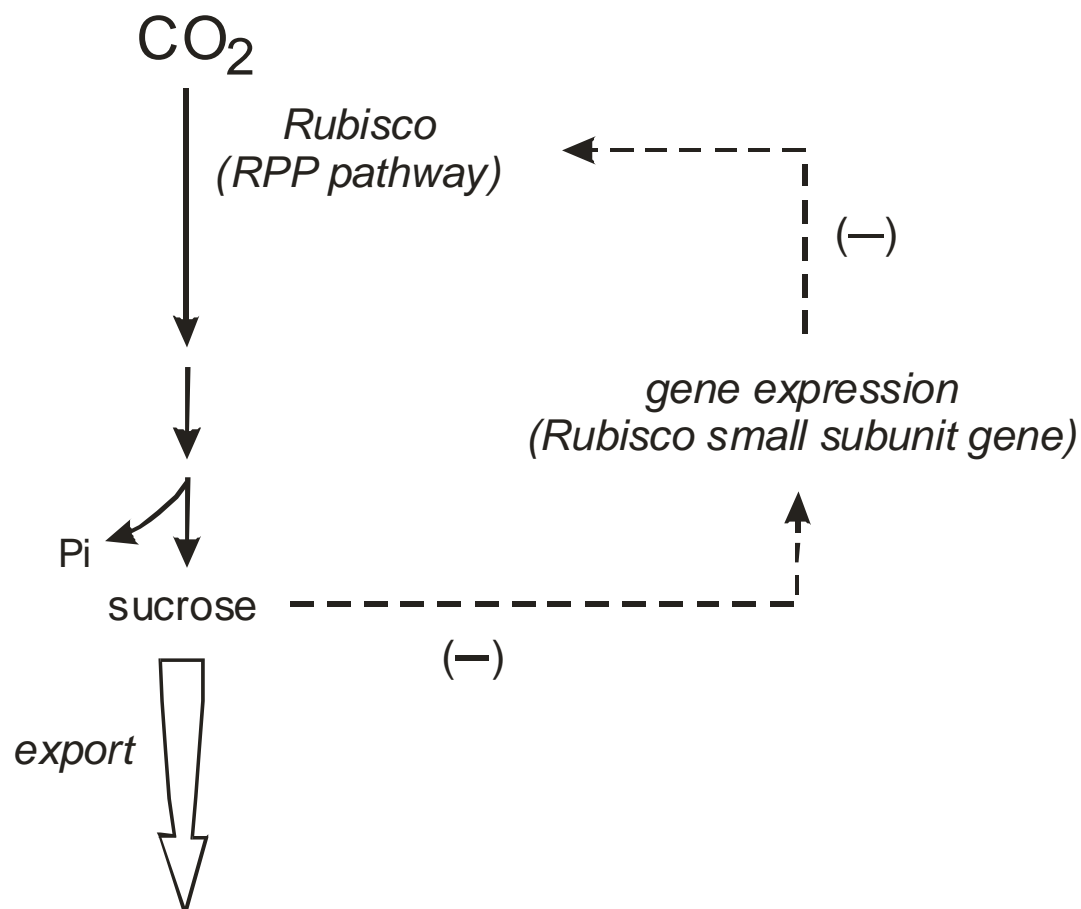


Figure B.4.1.2. Conceptual model showing negative feedback between sucrose concentration in a photosynthetic cell and expression of the gene for the small protein subunit of Rubisco. If the photosynthetic assimilation of CO_2 exceeds the capacity of the plant to accommodate the photosynthate (sucrose) that is produced, then the negative feedback loop will function to reduce the production of more Rubisco protein. As natural turnover of Rubisco occurs, the result will be a gradual reduction in Rubisco protein levels that permits better balance between the rates of photosynthetic CO_2 assimilation and photosynthate utilization.

Box 4.2 C₄ photosynthesis

Approximately 20% of the earth's gross primary productivity (GPP) is channeled through C₄ photosynthesis (Still et al. 2003). The fundamental advantage of C₄ photosynthesis is that Rubisco is localized within a special type of cell (the bundle-sheath cells), into which CO₂ is 'pumped' using an energy-driven metabolic process. This metabolic 'pumping' results in CO₂ concentrations in bundle-sheath cells that are several times higher than in the ambient atmosphere. Thus, in C₄ leaves, Rubisco exists in a cellular microenvironment that resembles the earth's primitive atmosphere of high CO₂ concentration. The elevated CO₂ concentration of bundle-sheath cells enhances the CO₂ assimilation rate by C₄ Rubisco, compared to C₃ Rubisco.

The C₄ pathway reflects coordinated metabolic function between two leaf cell types, mesophyll cells (MCs) and bundle-sheath cells (BSCs). Some of the key steps in C₄ photosynthesis include, (1) assimilation of inorganic carbon (as HCO₃⁻) in MCs by the enzyme phosphoenolpyruvate (PEP) carboxylase, (2) transfer of the resulting 4-C organic acids to the BSCs, (3) decarboxylation of the 4-C acids in the BSCs, (4) assimilation of the decarboxylated CO₂ by Rubisco, which is isolated to the BSCs, and (5) regeneration of a three-carbon CO₂ acceptor molecule by the expenditure of ATP energy in the MCs (Fig. B.4.2.1). In essence, ATP energy is used to transport CO₂ to the BSCs where it accumulates to relatively high concentrations (see Monson and Collatz 2009).

C₄ photosynthesis is most often found in the grasses of tropical and subtropical savannas, and in dicot species from hot, arid environments. In all cases, the CO₂-concentrating mechanism of the C₄ pathway facilitates high rates of CO₂ assimilation under conditions of high temperature and low CO₂ availability (due to drought and stomatal closure), both of which promote potentially high rates of photorespiration in C₃ plants. The C₄ CO₂-concentrating mechanism also provides C₄ plants with potentially higher rates of CO₂ assimilation per unit of N invested in Rubisco and per unit of water transpired (i.e., higher photosynthetic nitrogen- and water-use efficiencies, respectively).

A mathematical model of C₄ photosynthesis has been derived (von Caemmerer and Furbank 1999). The model is similar to that described for C₃ photosynthesis, in that it depends on the minimum of alternative constraints: in this case, the carboxylation-limited state (i.e., the limitation expressed by the capacity for PEP carboxylation in the MCs and RuBP carboxylation in the BSCs) and the electron transport-limited state (i.e., the limitation expressed by the

capacity to use ATP to regenerate RuBP in BSCs and the capacity to use ATP to regenerate PEP in MCs).

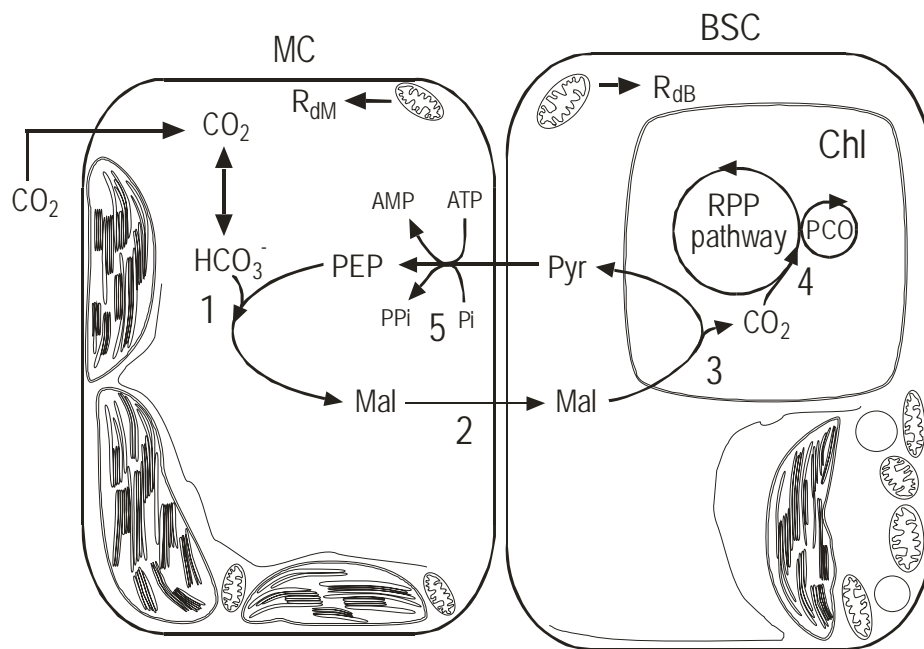


Figure B.4.2.1. The C₄ pathway of CO₂ assimilation as represented by a C₄ plant exhibiting the NADP-malic enzyme type of decarboxylation. 1, inorganic carbon is initially assimilated as HCO₃⁻ by the enzyme PEP carboxylase in the cytosol of the mesophyll cell (MC) (the equilibrium between CO₂ and HCO₃⁻ in the mesophyll cell is maintained by the enzyme carbonic anhydrase); 2, the 4-C dicarboxylic acid malate (Mal) is transported through plasmodesmatal connections to the bundle-sheath cell (BSC); 3, in this type of C₄ plant the malate is decarboxylated by the chloroplastic enzyme NADP-malic enzyme in the BSC; 4, the decarboxylated CO₂ is re-assimilated in the chloroplast (Chl) by Rubisco in the RPP pathway; 5, the 3-C product of decarboxylation, pyruvate (Pyr), is returned to the MC where ATP is used to produce phosphoenolpyruvate (PEP), the HCO₃⁻ acceptor molecule in the PEP carboxylase reaction. The C₄ cycle functions as a 'CO₂ pump' whereby ATP energy is used to 'pump' CO₂ into the BSC where it reaches concentrations several times higher than in the MC. This allows Rubisco (which is restricted to the BSC) to operate at higher CO₂ concentrations than in C₃ plants, and suppresses the activity of the photorespiratory carbon oxidation cycle, PCO). In essence, Rubisco is allowed to operate at CO₂ concentrations that more closely approximate those on a pre-Miocene earth, when atmospheric CO₂ concentrations were considerably higher than today. R_{dM} = mesophyll cell respiration due to the tricarboxylic acid cycle; R_{dB} = bundle-sheath cell respiration due to the tricarboxylic acid cycle.

Box 4.3 Stable isotope discrimination by Rubisco and at other points in plant carbon metabolism

The distribution of stable isotopes among different metabolite pools in a cell can provide insight into the kinetics of specific metabolic reactions, metabolic balance among different branches of connected pathways, and identification of rate limiting steps in a pathway. One of the well-studied sequences involving stable isotope fractionation within a metabolic context involves the movement of ^{13}C and ^{12}C , the two stable isotope forms of carbon, from the CO_2 reservoir in the atmosphere, through the sequential metabolite pools of photosynthesis and respiration, and back to the CO_2 reservoir in the atmosphere.

The assimilation of CO_2 in the photosynthetic reaction catalyzed by Rubisco exhibits a relatively large kinetic isotope effect favoring the assimilation of $^{12}\text{CO}_2$ relative to $^{13}\text{CO}_2$, $\alpha \approx 1.030$ ($\Delta \approx 30 \text{ ‰}$). The reaction sequence by which Rubisco catalyzes CO_2 assimilation is characterized by two sequential steps: (1) deprotonation of RuBP to form the reactive enediolate and, (2) covalent bond formation between the enediolate and the carbon of CO_2 . The kinetic isotope effect occurs during the second step in the reaction sequence, formation of the bond between the enediolate and CO_2 . There is some room for variation among the Rubiscos of different organisms in the magnitude of their kinetic isotope effect. The isotope effect will be slightly larger if the covalent bond forms late in the process of enediolate strain at the active site, thus reducing the probability of a reverse decarboxylation reaction (Tcherkez et al. 2006), or slightly smaller if the strength of the bond formed between the enediolate and CO_2 tends to be weaker, thus increasing the probability of a reverse decarboxylation reaction (McNevin et al. 2007). The actual discrimination expressed by Rubisco in C_3 leaves is considerably less than the theoretical maximum of 30 ‰ because of limitations in the capacity of unused $^{13}\text{CO}_2$ to diffuse away from the reaction site (see Section 3.D). Thus, the product of Rubisco-catalyzed CO_2 assimilation in C_3 plants exhibits a $^{13}\text{C}/^{12}\text{C}$ abundance ratio of $\sim 22\text{-}28 \text{ ‰}$ (explained by $\Delta = 14\text{-}20 \text{ ‰}$ *in vivo* combined with an atmospheric CO_2 $\delta^{13}\text{C}$ of -8 ‰).

Once assimilated by reactions of the RPP pathway, much of the carbon in triose phosphate sugars is oxidized through the processes of respiration in order to provide energy to the cell. The triose phosphate sugars are oxidized initially in the reactions of glycolysis, and finally in the mitochondrial reactions of the TCA cycle. The product of many of these oxidative steps is CO_2 .

If we assume that the initial distribution of ^{13}C and ^{12}C in the triose phosphate sugar molecules is random among the various C atoms, *and* there is no fractionation associated with respiratory processes, then there should be no difference in the $^{13}\text{C}/^{12}\text{C}$ ratio of photosynthetically-assimilated CO_2 and respired CO_2 . Thus, it was of interest when observations began to emerge showing that respired CO_2 was enriched in ^{13}C , relative to leaf sugars (Ghashghaie et al. 2003, Pataki 2005).

Some progress has been made in determining the causes of the ^{13}C enrichment in respired CO_2 . It turns out that the distribution of ^{13}C and ^{12}C in glucose molecules produced by photosynthesis is not random. For example, the carbon at position 4 in the glucose molecule tends to be enriched in ^{13}C , relative to the overall $^{13}\text{C}/^{12}\text{C}$ of assimilated carbon, while the carbon at position 6 tends to be depleted in ^{13}C (Rossman et al. 1991, Tcherkez et al. 2004). The cause of this non-random distribution is likely to be discrimination that favors ^{13}C in the aldolase reaction of the RPP pathway (Gleixner and Schmidt 1997). It is the carbon at position 4 that is lost as CO_2 in the initial step of mitochondrial respiration, resulting in the release of ^{13}C enriched CO_2 to the atmosphere. The two-carbon molecule that is left behind, following the loss of carbon 4 is depleted in ^{13}C , relative to the original glucose molecule. This molecule, known as acetyl Co-A, enters the TCA cycle, and is oxidized further. If all of the acetyl-CoA molecules were oxidized to CO_2 , there would be no overall enrichment in ^{13}C in respired CO_2 . This is because if all of a reactant is converted to product, there is no opportunity for a net isotope effect. In the case of acetyl-CoA, however, some of the molecules are used in metabolic pathways that branch off of the TCA cycle and are involved in the biosynthesis of lipids and other complex compounds, such as lignin. The carbon used in these branched pathways will be depleted in ^{13}C , relative to that lost from carbon 4 as respired CO_2 . As we gain more knowledge about the $^{13}\text{C}/^{12}\text{C}$ fractionation patterns in the various photosynthetic and respiratory pathways of a leaf, we will be able to better constrain the metabolic models that we produce to describe carbon partitioning in C_3 plants.

Footnotes (Chapter 2):

¹ To be faithful to the original derivation of Metabolic Control Analysis, we are using a change in enzyme concentration as the hypothetical perturbation required to quantify C_{Ex} . A change in enzyme activity could just as easily be used since enzyme concentration is proportional to enzyme activity under most conditions (see Kacser and Porteus 1987). In some studies of metabolic control analysis, genetically-engineered plants with variable enzyme concentrations have been produced and used to define C_{Ex} (see Stitt 1994).

² As an exercise in the application of Michaelis-Menten kinetics, and to better understand the foundation for Equation 4.7, the reader should attempt to understand that S_{rel} is the ratio of first-order dependencies of carboxylation rate on CO_2 concentration and oxygenation rate on O_2 concentration.

³ The same model logic can be used with respect to ATP; see Long and Bernacchi 2003.

⁴ Equation 3.17 is obtained after differentiation of $A = \frac{V_{\text{cmax}}(c_{\text{ci}} - \Gamma^*)}{c_{\text{ci}} + K_c(1 + c_{\text{oi}}/K_o)} - R_d$ with respect to c_{ci} , to obtain $\frac{dA}{dc_{\text{ci}}} = V_{\text{cmax}} \frac{\Gamma^* + K_c(1 + c_{\text{oi}}/K_o)}{[c_{\text{ci}} + K_c(1 + c_{\text{oi}}/K_o)]^2}$. The term $(c_{\text{ci}} - \Gamma^*)$ in the numerator of the first equation is intended to reflect the CO_2 diffusion gradient between the intercellular air spaces of the leaf and the chloroplast at the photocompensation point. At $c_{\text{ci}} \approx \Gamma^*$, Equation 4.17 is obtained.

⁵ The case has been made for adding a third category of respiratory CO_2 loss; that due to wastage (see Amthor 2000). Wastage refers to CO_2 that is released during the generation of energy and/or substrates that do not directly contribute to growth or maintenance. This would include futile cycles of ATP production and hydrolysis and the production of heat through the alternative respiration oxidase (cyanide-resistant pathway). Wastage respiration probably represents a minor CO_2 flux in most circumstances, as natural selection should favor efficiency, and it will not be explicitly considered in our further discussions.